Secretory modulation of basolateral membrane inwardly rectified K$^+$ channel in guinea pig distal colonic crypts

YINGJUN LI AND DAN R. HALM
Department of Physiology and Biophysics, Wright State University, Dayton, Ohio 45435

Li, Yingjun, and Dan R. Halm. Secretory modulation of basolateral membrane inwardly rectified K$^+$ channel in guinea pig distal colonic crypts. *Am J Physiol Cell Physiol* 282: C719–C735, 2002. First published October 24, 2001; 10.1152/ajpcell.00065.2001.—Cell-attached recordings revealed K$^+$ channel activity in basolateral membranes of guinea pig distal colonic crypts. Inwardly rectified currents were apparent with a pipette solution containing 140 mM K$^+$. Single-channel conductance (γ) was 9 pS at the resting membrane potential. Another inward rectifier with γ of 19 pS was observed occasionally. At a holding potential of -80 mV, γ was 21 and 41 pS, respectively. Identity as K$^+$ channels was confirmed after patch excision by changing the bath ion composition. From reversal potentials, relative permeability of Na$^+$ over K$^+$ (P_{Na}/P_K) was 0.02 ± 0.02, with $P_{Rb}/P_K = 1.1$ and $P_{Cl}/P_K < 0.03$. Spontaneous open probability (P_o) of the 9-pS inward rectifier ($^{gp}K_{ir}$) was voltage independent in cell-attached patches. Both a low ($P_o = 0.09 \pm 0.01$) and a moderate ($P_o = 0.41 \pm 0.01$) activity mode were observed. Excision moved $^{gp}K_{ir}$ to the medium activity mode; P_o of $^{gp}K_{ir}$ was independent of bath Ca^{2+} activity and bath acidification. Addition of Cl$^-$ and K$^+$ secretagogues altered P_o of $^{gp}K_{ir}$. Forskolin or carbachol (10 μM) activated the small-conductance $^{gp}K_{ir}$ in quiescent patches and increased P_o in low-activity patches. K$^+$ secretagogues, either epinephrine (5 μM) or prostaglandin E$_2$ (100 nM), decreased P_o of $^{gp}K_{ir}$ in active patches. This $^{gp}K_{ir}$ may be involved in electrogenic secretion of Cl$^-$ and K$^+$ across the colonic epithelium, which requires a large basolateral membrane K$^+$ conductance during maximal Cl$^-$ secretion and, presumably, a lower K$^+$ conductance during primary electrogenic K$^+$ secretion.

chloride secretion; potassium secretion; prostaglandin E$_2$; epinephrine

---

ACTIVE SECRETION OF IONS across colonic epithelia serves to produce a driving force for fluid secretion and to modify the composition of secreted fluid (7, 15). Excessive rates of secretion occur in pathophysiological states such as secretory diarrhea and ulcerative colitis. As in other fluid-secreting epithelia, electrogenic Cl$^-$ secretion is a major mechanism for producing fluid flow (14). Stimulating Cl$^-$ secretion requires exit of K$^+$ entering via the Na$^+$-K$^+$ pump and Na$^+$-K$^+$-2Cl$^-$ cotransport, which can occur via basolateral membrane K$^+$ channels (14). In mammalian colon, K$^+$ secretion is stimulated together with Cl$^-$ secretion, contributing to the relatively high luminal K$^+$ concentration. Localization studies support the presence of K$^+$ and Cl$^-$ secretory capacity in columnar cells of colonic crypts (18, 19). The cellular mechanism for K$^+$ secretion is electrogenic and related to the mechanism for Cl$^-$ secretion. A key feature is that electrogenic K$^+$ secretion measured in vitro is entirely bumetanide sensitive, suggesting an absolute requirement for Na$^+$-K$^+$-2Cl$^-$ cotransport (15, 41). In addition, apical and basolateral membrane K$^+$ channels allow exit of K$^+$ from the cell. Because the rate of K$^+$ secretion can vary relative to that of Cl$^-$ secretion, colonic secretory cells may control K$^+$ secretion, in part, by modulating basolateral K$^+$ channel activity to alter the amount of K$^+$ exiting into the lumen.

Activity of K$^+$ channels has been detected in colonic crypts (55), a site for fluid and mucus secretion (7, 16). Channels have been observed both in the crypt base (4, 5, 39) among the first progeny of the crypt stem cell and in the tubular portion of the crypt (32, 44, 45) among the rapidly dividing cells. The predominant cell types of the crypt are columnar cells and goblet cells (16, 19). Goblet cells are distinguished from columnar cells by dense apically located mucin granules that are released during cholinergic stimulation. Cl$^-$ secretion occurs with either cholinergic activation that increases intracellular Ca^{2+} or secretagogues such as vasoactive intestinal peptide and prostaglandin E$_2$ (PGE$_2$) that increase intracellular cAMP (7, 15). An increase in K$^+$ conductance would serve to maintain Cl$^-$ secretion by allowing K$^+$ exit and by developing a cell negative membrane electrical potential difference to drive conductive Cl$^-$ exit through the apical membrane into the lumen. Three major types of K$^+$ channels have been observed during secretory activation of isolated colonic crypts as well as colonic tumor cells such as T84 and HT29 (55): large-conductance, Ca^{2+}-activated K$^+$ channels (slo or BK); intermediate-conductance, Ca^{2+}-activated K$^+$ channels (IK1); small-conductance, cAMP-activated K$^+$ channels (KvLQT/minK). These K$^+$ channels belong to the greater group of K$^+$ channel proteins that have similar pore-forming domains but distinct regulatory domains and components (10, 27).

Guinea pig distal colon can produce high rates of K^+ and Cl^- secretion in response to secretagogues (17, 41). Both epinephrine and low concentrations of PGE_2 stimulate electrogenic K^+ secretion in the absence of accompanying Cl^- secretion, whereas high concentrations of PGE_2 or forskolin stimulate electrogenic secretion of both K^+ and Cl^-. Thus guinea pig distal colon provides a comparison between these two modes of secretion so that the varied roles of basolateral K^+ channels can be examined. In particular, increased basolateral membrane K^+ channel activity would aid Cl^- secretion by enhancing conductive Cl^- exit, whereas decreased activity would increase K^+ secretion by limiting exit of K^+ into the interstitial space. The present study has indicated that cells in colonic crypts exhibit an inwardly rectified K^+ channel, $^{gp}K_{ir}$, that has characteristics distinct from other K^+ channels previously observed in colonic epithelia. Both cAMP- and Ca^{2+}-dependent secretagogues activate $^{gp}K_{ir}$, whereas K^+ secretagogues moderate channel activity to lower levels.

METHODS

Male guinea pigs (400–650 g body wt) received standard guinea pig chow and water ad libitum. Guinea pigs were killed by decapitation in accordance with a protocol approved by the Wright State University Institutional Laboratory Animal Care and Use Committee. Distal colon was removed and defined as the ~20-cm-long segment ending roughly 5 cm from the rectum. Colonic segments were cut open along the mesenteric line and flushed with ice-cold Ringer solution to remove fecal pellets. Epithelium was separated from underlying submucosa and muscle layers by using a glass slide to gently scrape along the length of the colonic segment. The plane of dissection occurred at the base of the crypts such that only components of the mucosa immediately adherent to the epithelium remained. Portions of mucosa were mounted, with the use of cyanoacrylate glue, on to Lucite holders with apertures 1 cm wide and 4 cm long. Mucosal portions on holders were incubated at 38°C in HEPES-buffered solution with indomethacin (1 μM) to reduce spontaneous fluid and mucus secretion (16, 17, 41). Standard HEPES-buffered Ringer solution contained (in mM) 142 Na^+, 5 K^+, 2 Ca^{2+}, 1.2 Mg^{2+}, 143 Cl^-, 4 $H_{(3-X)}PO_4^{X-}$, 10 HEPES, and 10 D-glucose. Solutions were continually aerated with room air. Isolation of crypt epithelium from the mucosa followed general procedures developed previously (3, 5, 6, 44, 57). Solutions for separating epithelium from underlying connective tissue contained (in mM) 192 Na^+, 5 K^+, 97 Cl^-, 4 $H_{(3-X)}PO_4^{X-}$, 10 HEPES, 10 D-glucose, and either 30 mM citrate or EDTA. Isolation solution containing EDTA also had 0.1% bovine serum albumin. Best results were obtained if the EDTA solution was prepared the day of the isolation, as noted previously (3). Mucosal portions were consecutively incubated in 30 mM citrate Ringer with indomethacin (1 μM) for 15–30 min and then 30 mM EDTA Ringer for 15–20 min at 38°C. Holders were then gently agitated in HEPES-buffered Ringer with indomethacin (1 μM) and dithiothreitol (1 mM) to release surface and crypt epithelium. Inclusion of dithiothreitol reduced clumping of epithelium within extruded mucus. Isolated crypts were stored on ice or in the refrigerator until use and were suitable for patch-clamp experiments up to ~36 h.

Isolated crypts were transferred onto a polylysine-coated plastic coverslip in the electrical recording chamber mounted on the stage of an inverted microscope (Diaphot; Nikon, Tokyo, Japan). Bathing solutions were perfused into the chamber by a peristaltic pump (Gilson, Middleton, WI) at room temperature. Pipettes were fabricated from 7052 glass (WPI, Sarasota, FL) by using a two-stage puller (Narishige, Tokyo, Japan), coated with Q-dope (GC Electronics, Rockford, IL), and fire-polished. Pipettes filled with either high-Na^+ or high-K^+ solution (Table 1) had resistances of 5–10 MΩ and were connected to the head stage of an EPC-7 patch-clamp amplifier (List Medical, Darmstadt, Germany) via a 150 mM KCl agar salt bridge inside a holder containing a Ag-AgCl electrode (12). The reference electrode was a Ag-AgCl pellet connected to the bath through a 150 mM KCl agar salt bridge. Currents were recorded on videotape at 3-kHz filtering with a pulse code-modulated videocassette recorder (Vetter Instruments, Rebersburg, PA). Seals were made on the central tubular portion of isolated crypts bathed in standard HEPES-buffered Ringer solution. Seals of >1 GΩ were obtained in about one of five attempts. Occasionally, cell depolarization was produced with a high-K^+ bath made by substituting 135 mM K^+ for Na^+ in the standard Ringer solution. Before patches were excised, the bath solution was changed to one containing EGTA (Table 1) to maintain low free Ca^{2+} (~10 μM) that would mimic intracellular conditions. Lower levels of bath free Ca^{2+} (~100 nM and <10 nM free Ca^{2+}) were produced by adding only 0.1 mM or 0 mM Ca^{2+}, respectively, to these bath solutions. Bath solution pH was adjusted by titration with NaOH or HCl. Solution osmolarity was 292 mosM (290–294 mosM), except for the 300 KCl bath.

Drugs were added in small volumes from concentrated stock solutions. PGE_2 was obtained from Cayman Chemical (Ann Arbor, MI), and epinephrine was from Elkins-Sinn (Cherry Hill, NJ). All other chemicals were obtained from Sigma Chemical (St. Louis, MO). PGE_2 was prepared in an ethanol stock solution that added 0.1% ethanol at 10 μM PGE_2; additions of 1% ethanol alone did not alter transepithelial measures of K^+ or Cl^- secretion (17).

Table 1. *Patch-clamp solutions*

Solution	Na^+	K^+	Mg^{2+}	Ca^{2+}	Cl^-	Gluconate⁻	EGTA
High-Na^+ pipette	153	5	1.2	2.0	162		
High-K^+ pipette	18	140	1.2	2.0	162		
K-gluconate bath	14.5	143	5.0	1.0	50	114	1.0
Na-gluconate bath	157.5	0	5.0	1.0	50	114	1.0
70 mM K^+–85 mM Na^+ bath	85	70	5.0	1.0	161.5		1.0
300 mM KCl bath	5.5	300	5.0	1.0	312		1.0
RbCl bath	15	140Rb⁺	5.0	1.0	161.5		1.0

All solutions contained HEPES (5 mM) and were titrated to pH 7.4 for pipette and pH 7.2 for bath solutions.

Current data were transferred via DigiData-1200 interface to a computer for analysis using pCLAMP6 software (Axon Instruments, Foster City, CA). Currents were filtered at 700 Hz. Junction potentials at pipette tip and bath reference bridge were calculated to correct holding voltages (1, 38). Relative ion permeabilities were calculated by using the Goldman-Hodgkin-Katz potential equation together with the measured reversal potential and solution ion composition. Open probability (P_o) was calculated from all-points histograms of current amplitude. Area under each current peak (A) was determined by a Gaussian fit. P_o was obtained from the relation $P_o = [(\Sigma iA_i)/\Sigma A_i]/N$, with i indicating each peak starting at 0 for the baseline and increasing to N, the number of active channels. A current-voltage relation was constructed from the lowest current peaks to assure that the lowest peak at each voltage indicated the closed state. Records of sufficient length (5–10 min) were obtained for each stimulatory condition to allow a reliable measure of N from the number of observed peaks (22). Currents recorded at holding potentials (V_{hold}) more positive than about −10 mV were generally too small to allow accurate measurement of P_o. Kinetic analysis was performed on records containing only one channel by producing histograms of open and closed durations from an events list. For this analysis, current records were sampled

at a rate of 20 μs/point and then filtered at 1 kHz (Gaussian) to minimize noise but also to maximize bandwidth. Log binning was used to improve fitting and display of exponential curves (24); maximal likelihood estimates were used to obtain time constants from open and closed times. Results are reported as means ± SE. Statistical comparisons were made by using two-tailed Student's t-test for paired comparisons, with significant difference accepted at $P < 0.05$.

RESULTS

Basolateral membranes of isolated crypts were readily accessible to sealing with patch pipettes; all results were from seals on the middle (tubular) section of isolated crypts. Differences between columnar and goblet cells could not be discerned readily to identify the cell type recorded. Spontaneous single-channel currents were observed while cell-attached consistent with K⁺ channel activity (Fig. 1), with both high-Na⁺ and high-K⁺ pipette solutions (Table 1). The reversal potential in cell-attached recordings supported identification of channel types producing currents. For crypt epithelial cells (19, 31), currents from K⁺ and Cl⁻
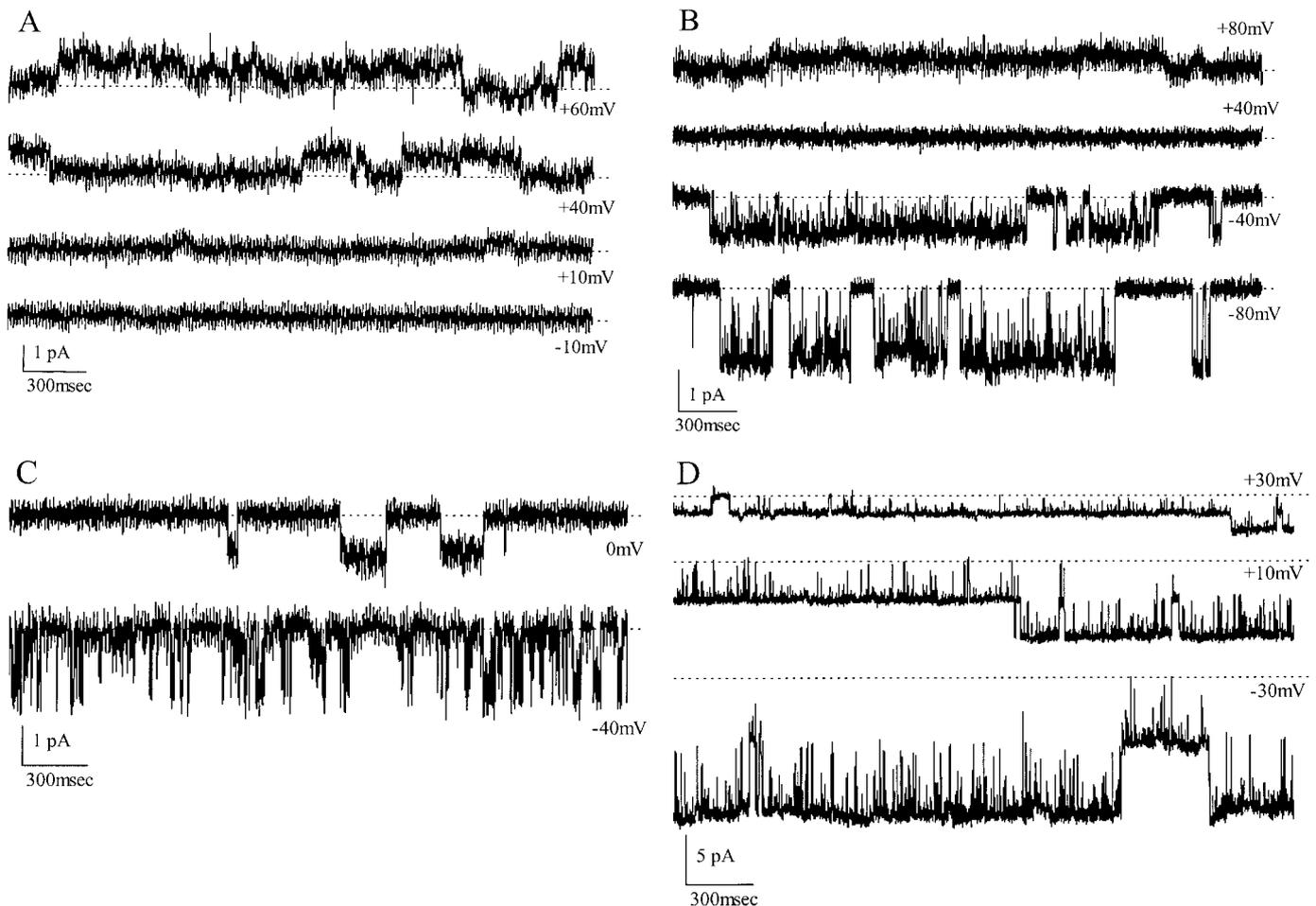

Fig. 1. K⁺ channel currents in crypt cells. Current traces are shown for K⁺ channels from cell-attached patches of basolateral membrane in isolated colonic crypts. Closed states are indicated by dashed lines. *A*: currents at several holding potentials (V_{hold}) are shown for an ~9-pS K⁺ channel with high-Na⁺ pipette solution, containing 5 mM K⁺ (see Table 1). *B*: currents for an inwardly rectified ~9-pS K⁺ channel with high-K⁺ pipette solution, containing 140 mM K⁺ (see Table 1). *C*: currents for a larger conductance (~19 pS) inwardly rectified K⁺ channel with high-K⁺ pipette solution. *D*: currents for an ~85-pS K⁺ channel with high-K⁺ pipette solution.

channels recorded with high-Na$^+$ pipette solution would be expected to reverse at negative and positive V_{hold}, respectively, as determined by the ion concentration gradients. Thus, at resting membrane electrical potential difference (V_{hold} = 0 mV), K$^+$ currents would be outward and Cl$^-$ currents would be inward (net outward Cl$^-$ flow). In addition, nonselective cation channel currents would reverse at large positive V_{hold}, corresponding to a cell membrane electrical potential difference of 0 mV. Use of high-K$^+$ pipette solution had the advantage of increasing the size of inward K$^+$ currents, thus permitting better detection of small-conductance channels. Because the equilibrium potential for K$^+$ would be near a membrane electrical potential difference of 0 mV with roughly equal K$^+$ concentrations inside and out, cell-attached reversal potentials of K$^+$ channel currents with high-K$^+$ pipette solution allowed a rough estimate of cell membrane electrical potential difference.

Currents consistent with Cl$^-$ channels, as distinguished by reversal potentials, also were observed (30). Nonselective cation channels (52) reversing at positive V_{hold} were not observed in cell-attached patches. Rarely (5 of 304 patches, 1.6%), nonselective cation channels were observed reversing at V_{hold} of 0 mV, suggesting a depolarization of membrane electrical potential difference for these cells. Changing the bath solution to a high-K$^+$ solution, which presumably depolarized cells, resulted occasionally (9 of 57 patches,

16%) in the appearance of nonselective cation channels in cell-attached patches. For patches with nonselective cation channels, two to six channels were present with a voltage-independent single-channel conductance of ~25 pS.

The most common K$^+$ channel activity with high-Na$^+$ pipette solution (10 of 73 patches, 14%) had a linear current-voltage relation with a single-channel conductance (γ) of 9 pS (Figs. 1A and 2). During recording with high-K$^+$ pipette solution, inwardly rectified current-voltage relations were observed (58 of 231 patches, 25%) with γ of 9 and 19 pS at V_{hold} = 0 mV (Figs. 1, B and C, and 2). These two channel behaviors with high-K$^+$ pipette solution may be specific conductance states of the same channel, because they were observed together (3 of 6 patches with large-conductance ^{gp}K$_{ir}$, 50%). Cell-attached currents consistent with a K$^+$ channel of ~85 pS also were seen in one patch with the standard bath solution (Figs. 1D and 2A) and in one other patch with high-K$^+$ bath solution that presumably depolarized cells. Apparent higher incidence of K$^+$ channels with high-K$^+$ pipette solution may only reflect the generally greater ease of identifying the resulting larger inward K$^+$ currents.

Ion selectivity of ^{gp}K$_{ir}$. Activity of ^{gp}K$_{ir}$ generally persisted after excision into an inside-out (I/O) configuration (17 of 18 patches, 94%), which allowed ion selectivity to be determined more precisely. With a high-K$^+$ pipette solution and a K-gluconate bath solu-
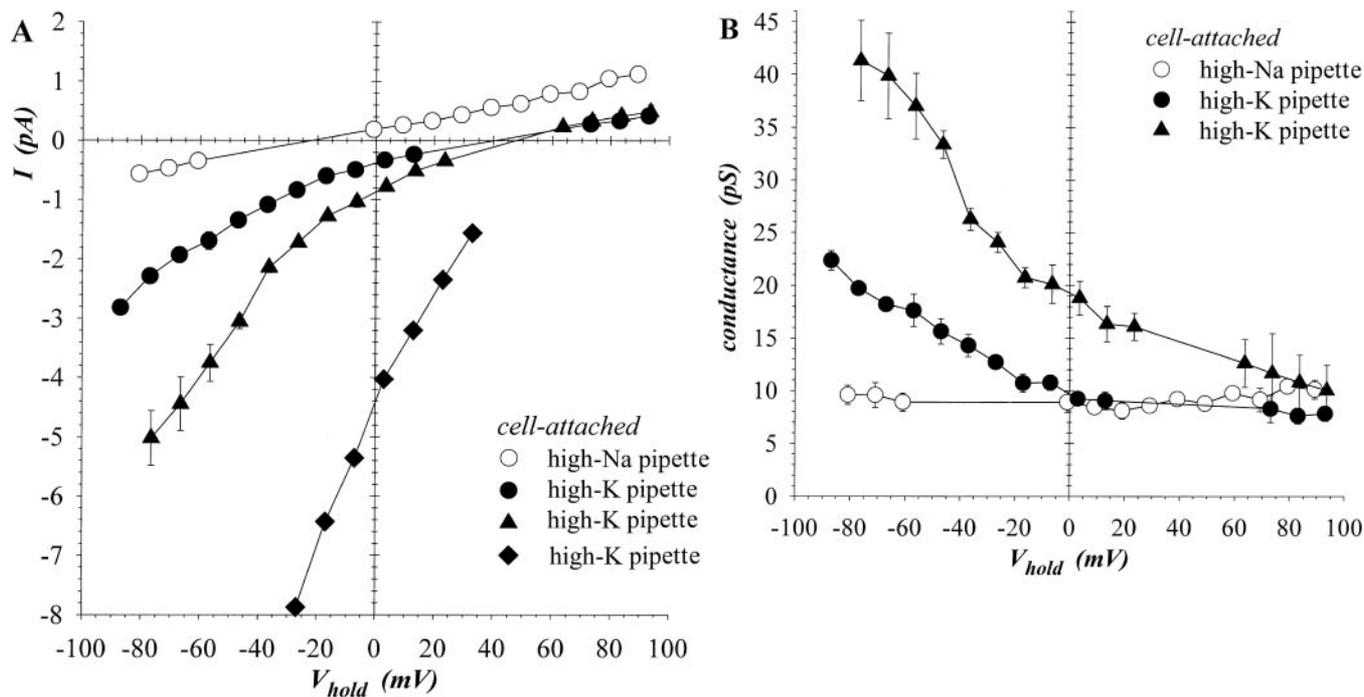

Fig. 2. K$^+$ channel conductive properties. *A*: current-voltage relations are shown for 4 types of K$^+$ channel activity observed in cell-attached patches of crypt basolateral membrane (means ± SE). With high-Na$^+$ pipette solution, single-channel currents were linearly dependent on voltage ($\circ$, n = 6). With high-K$^+$ pipette solution, currents were inwardly rectified, and those exhibiting both inward and outward currents were averaged ($\bullet$, n = 15). Larger inwardly rectified currents forming a distinct group were averaged ($\blacktriangle$, n = 6). A larger conductance (~85 pS) K$^+$ channel recorded with high-K$^+$ pipette solution also is shown ($\blacklozenge$, n = 1). Symbols often obscure small error bars. *I*, current. *B*: single-channel conductance (chord conductance, γ) is shown from current-voltage relations in *A*.

tion (containing 50 mM Cl$^-$, Table 1), the reversal potential was near 0 mV (Fig. 3A), as expected for a cation channel. Increasing bath solution KCl concentration shifted the reversal potential to negative voltages (Fig. 3A) consistent with cation selectivity. Relative anion permeability (P_{Cl}/P_K) was <0.03 ($n = 9$). Lowering bath solution K$^+$ concentration by substitution with Na$^+$ shifted the reversal potential to positive voltages, as expected for a K$^+$-selective channel (Fig. 3A). Relative Na$^+$ permeability (P_{Na}/P_K) was 0.02 ± 0.02 ($n = 6$). Substituting bath K$^+$ completely with Na$^+$ produced steep inwardly rectified currents without outward currents (Fig. 3C), also consistent with high selectivity for K$^+$ over Na$^+$. Similarly (Fig. 3A), relative Rb$^+$ permeability (P_{Rb}/P_K) was 1.12 ($n = 2$, range 1.05–1.19). Currents from the 9-pS channel with high-Na$^+$ pipette and Na-gluconate bath solution also were completely inwardly rectified (Fig. 3C), supporting identification as a K$^+$ channel. Ion selectivity of the 19-pS ^{gp}K$_{ir}$ also supported high preference for K$^+$ over Na$^+$ or Cl$^-$ (data not shown). These current measurements indicate that the observed channels were K$^+$ selective with significant Rb$^+$ permeability, suggesting a divergence from other inwardly rectified K$^+$ channels (8, 49).

Concentration dependence of ^{gp}K$_{ir}$. Increasing K$^+$ concentration at the cytoplasmic face of the patch (0, 70, and 143 mM; with constant ionic strength) increased γ of ^{gp}K$_{ir}$ at positive membrane potentials (V_m) (Fig. 3D), consistent with saturation of outward flow at <70 mM K$^+$. Further increase of K$^+$ concentration to 300 mM (with increased ionic strength) led to ~45% larger γ at positive V_m (Fig. 3B). For inward K$^+$ flow from the pipette, decreasing K$^+$ concentration in the bath (with constant ionic strength) did not alter γ at large negative V_m (Fig. 3D), but high bath K$^+$ concentration (300 mM; with higher ionic strength) increased γ at negative V_m (Fig. 3B). One possible explanation for this apparent influence of cytoplasmic K$^+$ on K$^+$ influx, and efflux, is that the small-conductance state of ^{gp}K$_{ir}$ was converted to the large-conductance state by increased ionic strength, since γ at negative V_m with 300 mM bath K$^+$ (Fig. 3B) was similar to γ of the large-conductance ^{gp}K$_{ir}$ (Fig. 2B).

During cell-attached recording with high-Na$^+$ pipette solutions (Fig. 2), outward rectification was not apparent for the 9-pS K$^+$ channel even though pipette K$^+$ concentration was only 5 mM (Table 1). Lack of outward rectification with an outwardly directed concentration gradient suggests that this K$^+$ channel actually was an inward rectifier, similar to previous observations on colonic K$^+$ channels (39). Relative Rb$^+$ conductance of ^{gp}K$_{ir}$ was similar to that with K$^+$ (Fig. 3B), indicating that the mechanism producing rectification (27) apparently was not altered appreciably by Rb$^+$ substitution for K$^+$ at the cytoplasmic face of the channel. Similarity of K$^+$ efflux with high-Na$^+$ and high-K$^+$ pipette solutions, as indicated by γ at positive V_{hold} (Fig. 2B), supports the suggestion that these two K$^+$ channel activities (Fig. 1, A and B) were an identical channel type, an inward rectifier.

Voltage dependence of γ for ^{gp}K$_{ir}$. Excision into an I/O configuration can lead to altered channel behavior as cytoplasmic components are lost. Single-channel conductance of ^{gp}K$_{ir}$ was not changed dramatically by excision into a high-K$^+$ solution that mimicked intracellular ion composition (Figs. 2B and 3B). Generally the small-conductance state was present, although the large-conductance state was observed (2 of 18 patches, 11%). However, a direct comparison of conductance-voltage dependence for cell-attached and excised conditions requires an estimate of resting cell membrane electrical potential difference (V_{cell}). Assuming that cell-attached reversal potentials of K$^+$ channels with high-K$^+$ pipette solution represented a V_{cell} of 0 mV, cell-attached V_{hold} then can be adjusted to indicate actual V_m (Fig. 3E). Excised γ appeared to conform best in size to the small-conductance state seen with cell-attached recordings. The ~50 mV rightward shift in voltage dependence for γ indicates that cytoplasmic factors controlling γ may have been lost upon excision. One possibility is that Mg^{2+} in the bath solution (Table 1) during I/O conditions blocks ^{gp}K$_{ir}$ with different voltage dependence than the native cytoplasmic components (27).

Kinetic modes of ^{gp}K$_{ir}$. P_o of ^{gp}K$_{ir}$ during cell-attached recording was voltage independent but occurred in two distinct modes (Fig. 4A), moderate activity ($P_o = 0.41 ± 0.01$, $n = 8$) and low activity ($P_o = 0.09 ± 0.01$, $n = 6$). Abrupt transitions between low and moderate states were observed (4 of 58 patches with ^{gp}K$_{ir}$, 7%) but were not reversed, suggesting that a voltage-independent regulatory process controlled transitions between these two kinetic modes of ^{gp}K$_{ir}$. Excision into an I/O configuration increased P_o of low-activity ^{gp}K$_{ir}$, producing a kinetic mode with brief open and closed events (Fig. 4B); transition to moderate P_o occasionally occurred only several minutes after excision. In the excised I/O condition, P_o was similar to the moderate-activity state ($P_o = 0.42 ± 0.01$, $n = 5$) regardless of whether cell-attached activity had been low or moderate (Fig. 4C), indicating that excision may remove a cytoplasmic component that acts to limit P_o.

Secretagogue modulation of ^{gp}K$_{ir}$ activity. Numerous secretagogues stimulate electrogenic K$^+$ and Cl$^-$ secretion across distal colonic epithelia (7, 15). Electrogenic K$^+$ secretion is stimulated by epinephrine or PGE$_2$, and at higher concentrations PGE$_2$ stimulates Cl$^-$ and K$^+$ secretion (17, 41). In addition, the cholinergic agonist carbachol (CCh) stimulates Cl$^-$ secretion. Forskolin, which increases intracellular cAMP through activation of adenylate cyclase, also stimulates electrogenic Cl$^-$ secretion. Spontaneous activity of ^{gp}K$_{ir}$ was observed with both high-Na$^+$ (7 of 10 patches with ^{gp}K$_{ir}$, 70%) and high-K$^+$ pipettes (42 of 58 patches with ^{gp}K$_{ir}$, 72%). Addition of forskolin to the bath during cell-attached recording increased both the number of open ^{gp}K$_{ir}$ (N) and apparent P_o in quiescent patches (Figs. 5A and 7A) and in patches with spontaneous activity (Figs. 6A and 7B). CCh added to the bath during cell-attached recording also activated ^{gp}K$_{ir}$ in a quiescent patch (Fig. 5B).
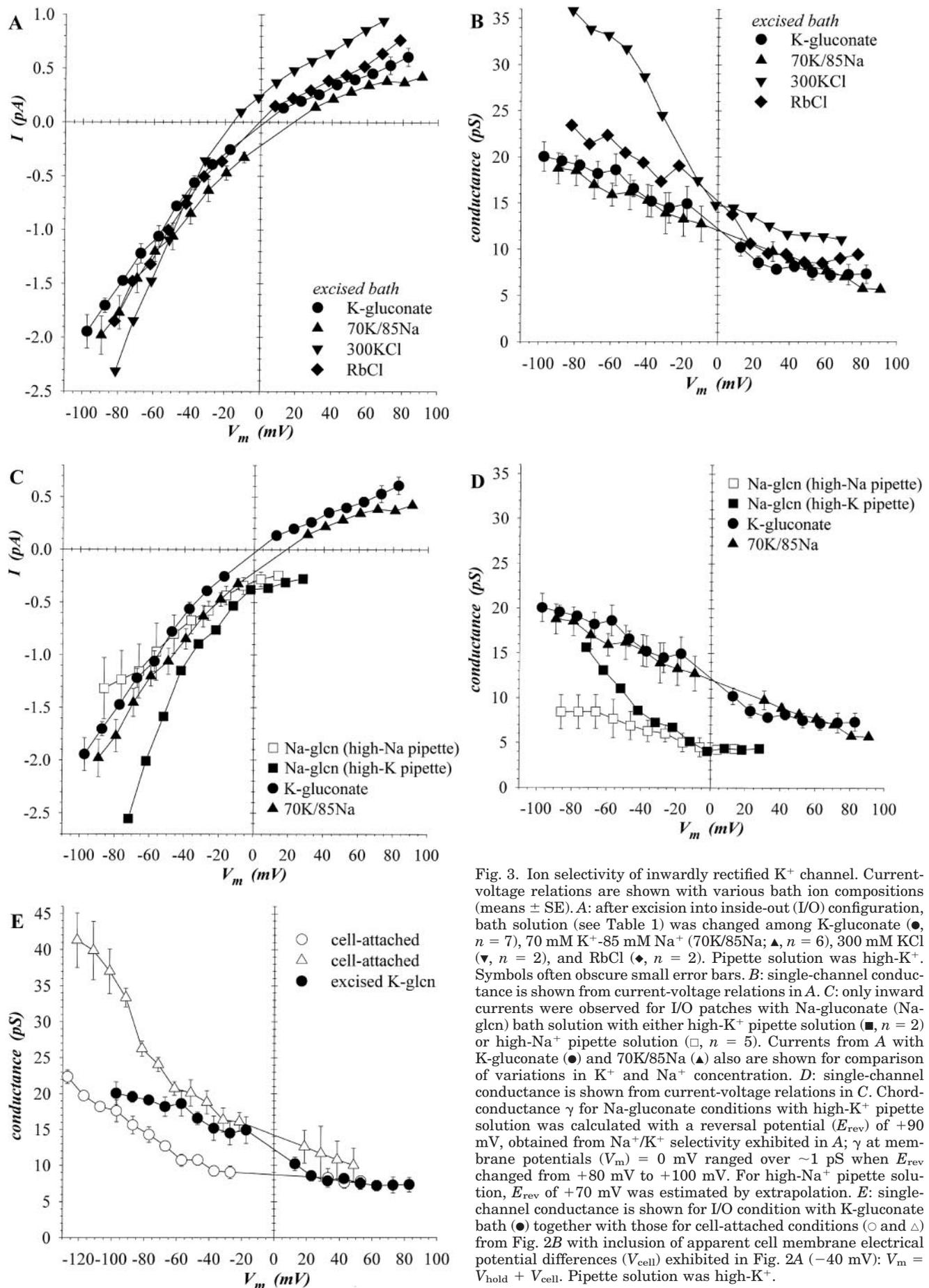
Fig. 3. Ion selectivity of inwardly rectified K⁺ channel. Current-voltage relations are shown with various bath ion compositions (means ± SE). *A*: after excision into inside-out (I/O) configuration, bath solution (see Table 1) was changed among K-gluconate (●, $n = 7$), 70 mM K⁺-85 mM Na⁺ (70K/85Na; ▲, $n = 6$), 300 mM KCl (▼, $n = 2$), and RbCl (◆, $n = 2$). Pipette solution was high-K⁺. Symbols often obscure small error bars. *B*: single-channel conductance is shown from current-voltage relations in *A*. *C*: only inward currents were observed for I/O patches with Na-gluconate (Na-glcn) bath solution with either high-K⁺ pipette solution (■, $n = 2$) or high-Na⁺ pipette solution (□, $n = 5$). Currents from *A* with K-gluconate (●) and 70K/85Na (▲) also are shown for comparison of variations in K⁺ and Na⁺ concentration. *D*: single-channel conductance is shown from current-voltage relations in *C*. Chord-conductance γ for Na-gluconate conditions with high-K⁺ pipette solution was calculated with a reversal potential (E_{rev}) of +90 mV, obtained from Na⁺/K⁺ selectivity exhibited in *A*; γ at membrane potentials (V_m) = 0 mV ranged over ~1 pS when E_{rev} changed from +80 mV to +100 mV. For high-Na⁺ pipette solution, E_{rev} of +70 mV was estimated by extrapolation. *E*: single-channel conductance is shown for I/O condition with K-gluconate bath (●) together with those for cell-attached conditions (○ and △) from Fig. 2*B* with inclusion of apparent cell membrane electrical potential differences (V_{cell}) exhibited in Fig. 2*A* (−40 mV): $V_m = V_{hold} + V_{cell}$. Pipette solution was high-K⁺.
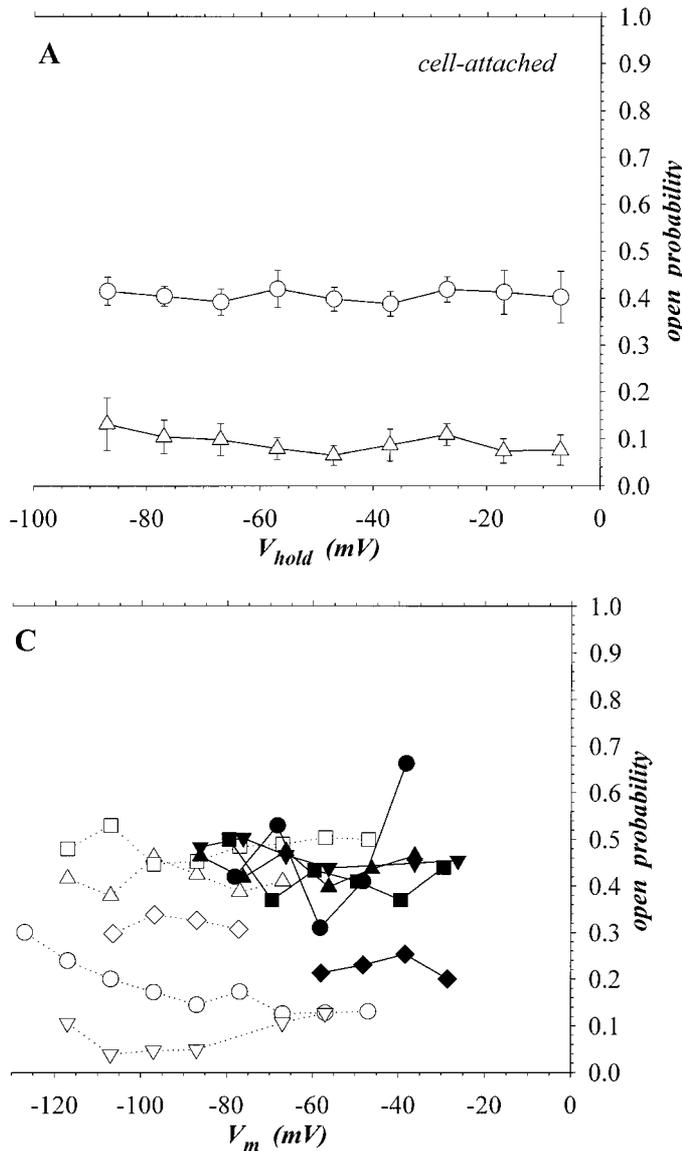
Fig. 4. Open probability (P_o) of guinea pig inward rectifier K$^+$ channel (^{gp}K$_{ir}$). Currents from ^{gp}K$_{ir}$ were recorded before and after excision into I/O configuration. P_o was calculated from current records (see METHODS). Pipette solution was high-K$^+$. A: dependence of P_o on V_{hold} is shown for cell-attached condition (means ± SE). Spontaneous activity was observed in either of 2 states, moderate ($\circ$, $n = 8$) or low ($\triangle$, $n = 6$). B: a cell-attached patch was excised into K-gluconate bath solution. Current traces are shown for V_{hold} of -50 mV. Closed states are indicated by dashed lines. Openings for 2 ^{gp}K$_{ir}$ were apparent after excision. C: P_o is shown for those patches ($n = 5$) in which ^{gp}K$_{ir}$ from basal conditions were recorded in both cell-attached (open symbols) and excised I/O (filled symbols) configurations. Cell-attached P_o is shown with inclusion of apparent V_{cell}, -40 mV (see Fig. 2A).

Using epinephrine to produce a K$^+$ secretory state decreased apparent P_o of forskolin-stimulated ^{gp}K$_{ir}$ (Figs. 5A and 7B) and of spontaneously active ^{gp}K$_{ir}$ (Fig. 6B). PGE$_2$ reduced apparent P_o after forskolin stimulation (Fig. 6A) and in the presence of epinephrine (Fig. 6B and 7B); forskolin addition in the presence of epinephrine and PGE$_2$ modestly increased apparent P_o, though not to basal level (Fig. 6B). In a patch with low apparent P_o stimulated by forskolin (Fig. 7A), PGE$_2$ addition led to complete inactivation of ^{gp}K$_{ir}$. A patch with a single ^{gp}K$_{ir}$ (Fig. 7B) exhibited progressive modulation of P_o during cumulative addition of secretagogues, increase with forskolin, decrease with epinephrine, and further decrease with PGE$_2$.

Forskolin and CCh, which activate Cl$^-$ secretion, generally increased N and P_o of ^{gp}K$_{ir}$, whereas epinephrine and PGE$_2$, which activate K$^+$ secretion, generally decreased N and P_o (Figs. 5–7). Forskolin activated ^{gp}K$_{ir}$ (increased N) in quiescent patches (10 of 80 patches, 12.5%); CCh also increased N of ^{gp}K$_{ir}$ (4 of 43

quiescent patches, 9%). PGE$_2$ did not activate ^{gp}K$_{ir}$ (0 of 30 quiescent patches); epinephrine rarely activated ^{gp}K$_{ir}$ (2 of 57 quiescent patches, 3%). These observed proportions of ^{gp}K$_{ir}$ activation include secretagogue additions to patches that may not have contained ^{gp}K$_{ir}$ so that actual efficacy may have been higher. Comparisons among these secretagogue results, however, do provide a relative assessment of action on ^{gp}K$_{ir}$, because all patches were sampled from the same group of crypts.

Secretagogue actions also were compared for patches containing spontaneously active ^{gp}K$_{ir}$, which eliminated the confounding effect of blank patches. Forskolin activated additional ^{gp}K$_{ir}$ in patches with spontaneously active ^{gp}K$_{ir}$ (3 of 12 active patches, 25%); CCh did not activate ^{gp}K$_{ir}$ in patches with spontaneously active ^{gp}K$_{ir}$ (0 of 6 active patches). Both epinephrine (2 of 12 active patches, 17%) and PGE$_2$ (4 of 17 active patches, 23%) inactivated ^{gp}K$_{ir}$ in patches with spontaneously active ^{gp}K$_{ir}$; these K$^+$ secretagogues did not
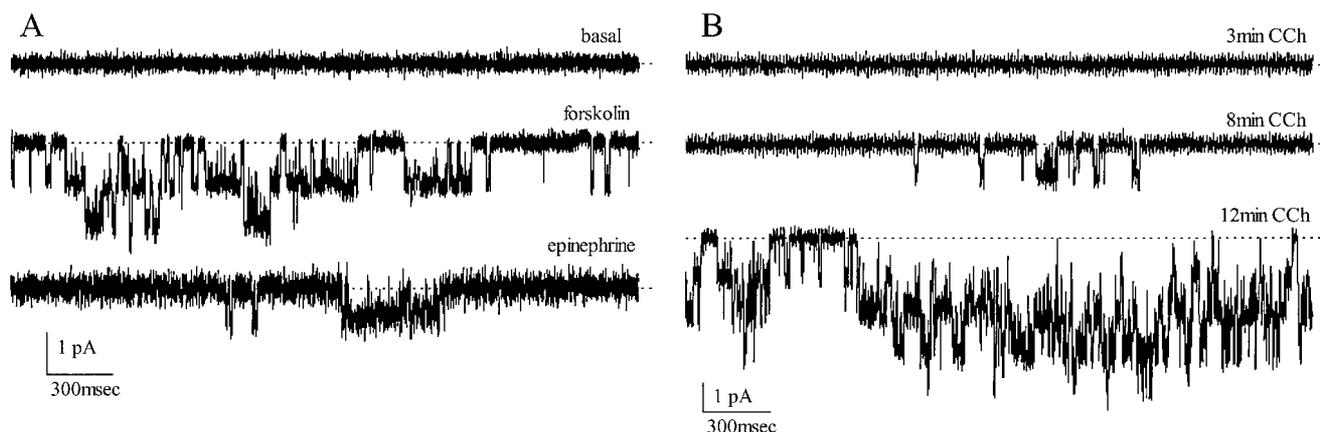
Fig. 5. Secretagogue activation of $^{gp}K_{ir}$. Currents from $^{gp}K_{ir}$ were recorded during cumulative addition of secretagogues to spontaneously quiescent patches. Activity generally was recorded at 10-mV increments of V_{hold}. Pipette solution was high-K⁺. Closed states are indicated by dashed lines. *A*: a cell-attached patch was sequentially treated with forskolin (1 µM) and epinephrine (5 µM). Currents are shown 10.8 min after forskolin addition for V_{hold} of −60 mV and 6.5 min after epinephrine addition for V_{hold} of −50 mV; because P_o was voltage independent (see Fig. 4*A*), kinetic changes can be assessed from these current traces. The number of open $^{gp}K_{ir}$ increased to 3 with forskolin. *B*: a cell-attached patch was treated with carbachol (CCh; 10 µM) for V_{hold} of −50 mV. Time after addition of CCh is noted. The number of open $^{gp}K_{ir}$ increased to 7 with CCh.

activate further $^{gp}K_{ir}$ in active patches. Large-conductance $^{gp}K_{ir}$ (Figs. 1*C* and 2) also were activated by forskolin (4 of 6 patches with large-conductance $^{gp}K_{ir}$ recorded, 67%); other secretagogues did not activate this large-conductance $^{gp}K_{ir}$. These proportions for secretagogue action may include some patches with every $^{gp}K_{ir}$ present already activated such that further increases in N were not possible. In addition, these spontaneously active patches may have been in a state that altered sensitivity to secretagogues.

Secretagogue-induced changes in P_o and N for $^{gp}K_{ir}$, similar to the patches shown in Figs. 5–7, are summarized in Fig. 8. P_o remained independent of V_{hold} after addition of forskolin, CCh, epinephrine, or PGE₂ (Fig.

8*C*). Forskolin and CCh, on average, increased P_o to a level (0.38 ± 0.10, $n = 8$, and 0.28 ± 0.05, $n = 3$, respectively) consistent with the moderate-activity mode of spontaneously active patches (Fig. 4*A*). PGE₂ and epinephrine, on average, decreased P_o to a level (0.22 ± 0.04, $n = 10$, and 0.21 ± 0.07, $n = 6$, respectively) between the two activity modes of spontaneously active patches (Fig. 4*A*). Some of the variation in secretagogue responses may depend on the order of secretagogue addition, the cell type sealed, and the prior, unknown state of each crypt. Epinephrine once activated $^{gp}K_{ir}$ ($N = 3$, Fig. 8*B*) only after forskolin had failed to stimulate a quiescent patch, and P_o increased only to ~0.1 (Fig. 8*A*), similar to the low-activity mode
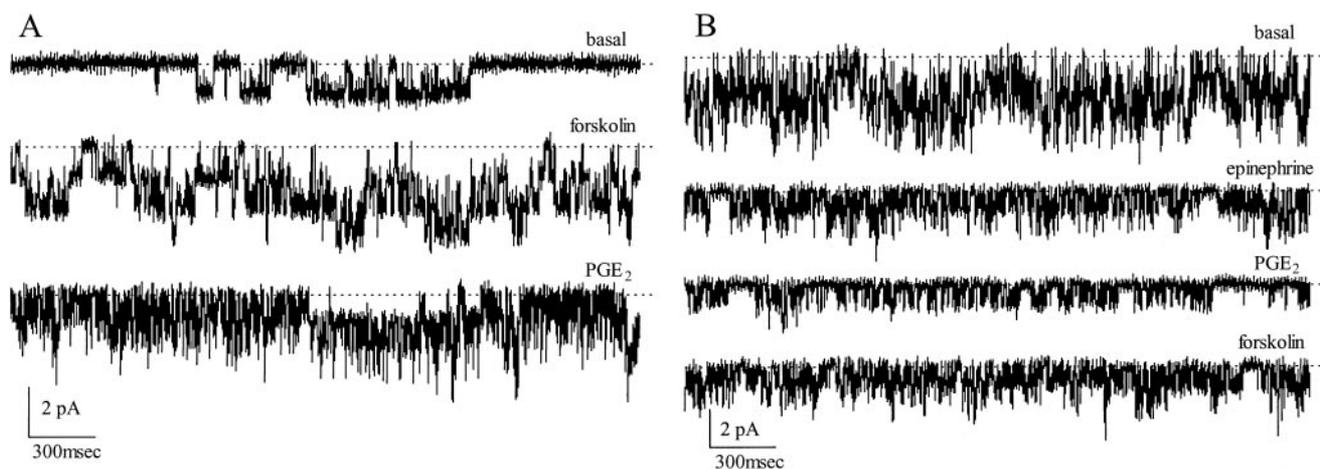

Fig. 6. Secretagogue modulation of $^{gp}K_{ir}$. Currents from spontaneously active $^{gp}K_{ir}$ were recorded during cumulative addition of secretagogues. Pipette solution was high-K⁺. Closed states are indicated by dashed lines. *A*: a cell-attached patch was sequentially treated with forskolin (10 µM) and PGE₂ (10 µM) for V_{hold} of −50 mV. Currents are shown 13.0 min after forskolin addition and 11.7 min after PGE₂ addition. The number of open $^{gp}K_{ir}$ increased from 1 in basal to 4 with forskolin and PGE₂. *B*: a cell-attached patch was sequentially treated with epinephrine (5 µM), PGE₂ (10 µ), and forskolin (10 µM) for V_{hold} of −60 mV. Currents are shown 12.8 min after epinephrine addition, 9.3 min after PGE₂ addition, and 8.7 min after forskolin addition. The apparent number of open $^{gp}K_{ir}$ in basal was 5.
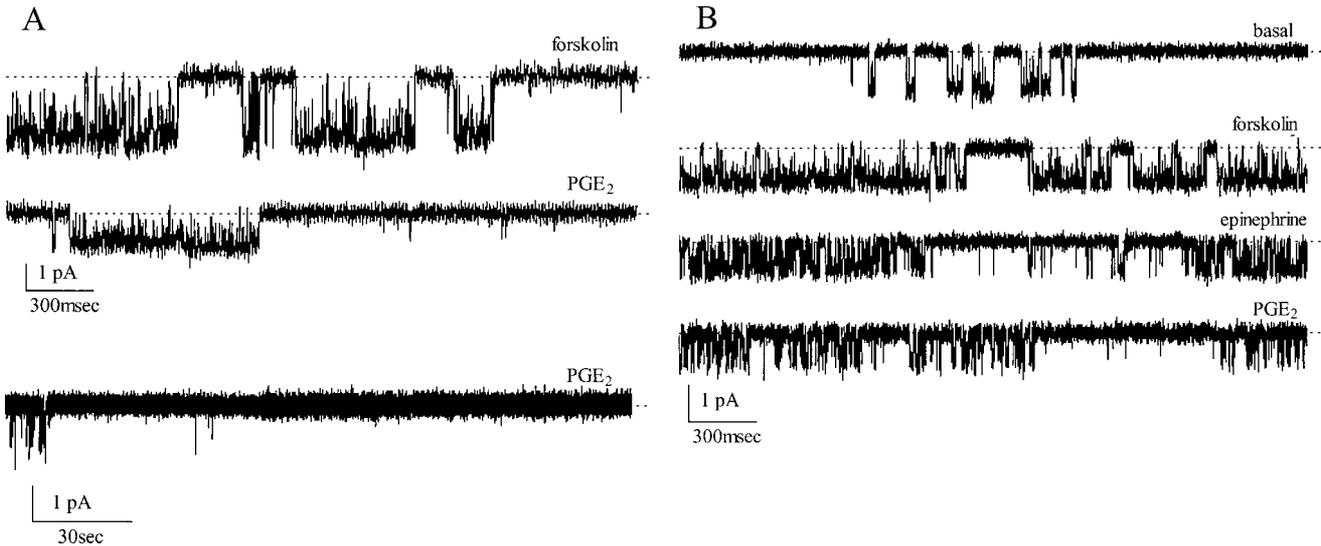
Fig. 7. Secretagogues reduce activity of $^{gp}K_{ir}$. Currents from $^{gp}K_{ir}$ were recorded during cumulative addition of secretagogues. Pipette solution was high-K$^+$. Closed states are indicated by dashed lines. *A*: a cell-attached patch in which CCh (10 μM) had failed to activate $^{gp}K_{ir}$ after ~20 min was sequentially treated with forskolin (10 μM) and PGE$_2$ (10 μM) (*upper traces*). Currents are shown ~19 min after forskolin addition for V_{hold} of −80 mV and ~20 s after PGE$_2$ addition for V_{hold} of −40 mV. P_o was 0.01 ± 0.001 during forskolin treatment. Open $^{gp}K_{ir}$ inactivated after ~1 min with PGE$_2$ (*lower trace*) such that activity at other V_{hold} was not obtained. *B*: a cell-attached patch was treated sequentially with forskolin (1 μM), epinephrine (5 μM), and PGE$_2$ (100 nM) for V_{hold} of −50 mV. Currents are shown 18.5 min after forskolin addition, 17.4 min after epinephrine addition, and 17.6 min after PGE$_2$ addition. Only 1 $^{gp}K_{ir}$ was open throughout treatment; P_o was 0.05 ± 0.02 (basal), 0.71 ± 0.02 (forskolin), 0.46 ± 0.02 (epinephrine), and 0.34 ± 0.01 (PGE$_2$).

of spontaneously active patches (Fig. 4A). Forskolin produced the smallest P_o increases when in the presence of other secretagogues or with P_o near 1.0. Increasing PGE$_2$ concentration from 100 nM to 10 μM did not lead to further change in P_o (from 0.27 ± 0.04 to 0.24 ± 0.07, paired difference −0.03 ± 0.04, $n = 3$). P_o and N changed in a manner consistent with the expected demands of transepithelial ion secretion, increasing during Cl$^-$ secretion and decreasing during K$^+$ secretion.

Kinetic mechanism of $^{gp}K_{ir}$. Open and closed durations of $^{gp}K_{ir}$ activity were examined to obtain a preliminary mechanism controlling P_o changes by secretagogues. Histograms of open durations from a patch containing a single $^{gp}K_{ir}$ (Fig. 7B) exhibited one peak. In the basal and forskolin condition, the peak was fit well by one exponential, and after K$^+$ secretagogue additions, two exponentials were required for an adequate fit (Fig. 9, *A–D*) consistent with at least two open states for $^{gp}K_{ir}$. Histograms of closed durations exhibited several peaks, indicating multiple closed states for $^{gp}K_{ir}$ (Fig. 9, *E–H*). Closed durations for the basal condition were fit well by four exponentials (Fig. 9E) with widely separated time constants, indicating at least four closed states for spontaneously active $^{gp}K_{ir}$. Closed durations during forskolin, epinephrine, and PGE$_2$ addition also were fit best by four exponentials (Fig. 9, *F–H*), indicating at least four closed states for secretagogue-stimulated conditions. Forskolin stimulation of P_o (Fig. 8A) occurred through elimination of closed events longer than ~400 ms with a small relative increase in closed events of intermediate duration

(Fig. 9F). Reduction of P_o by epinephrine and PGE$_2$ occurred through a further increase in the number of closed events of intermediate duration (Fig. 9, *G* and *H*) and a decrease of time constants for open events (Fig. 9, *C* and *D*). Activation of $^{gp}K_{ir}$ appears to have occurred largely by altering residence in various closed states, which can be seen qualitatively in the current records (Figs. 5–7). Modulation of P_o at intermediate levels also occurred through changes of relative residence in closed states, together with shortening of the longer open time constant.

The kinetic mechanism for $^{gp}K_{ir}$ was analyzed further with other patches containing only one active channel; 10 $^{gp}K_{ir}$ were examined from 16 fits for conditions including spontaneous activity, secretagogue stimulation, and excision. One open state was apparent in basal conditions with low P_o, as judged by open-duration histograms fit by a single exponential (8.0 ± 0.6 ms, $n = 3$). Spontaneously active $^{gp}K_{ir}$ in the medium-P_o mode ($n = 3$) had open-duration histograms fit by two exponentials with time constants 0.8 ± 0.2 ms (32 ± 11%) and 2.6 ± 0.1 ms (68 ± 11%). These two time constants further support the presence of at least two open states for $^{gp}K_{ir}$ (Fig. 10A), a short-duration state (O$_S$) and a longer duration state (O$_L$). Fits of closed-duration histograms from various conditions suggest the presence of at least five closed states, even though many were fit well individually by four exponentials.

Closed time constants clustered into six distinct groups (Fig. 10B). All of the $^{gp}K_{ir}$ examined had a component with a time constant in the first group, C$_1$. Many $^{gp}K_{ir}$ (7 of 10) also had contributions in the next
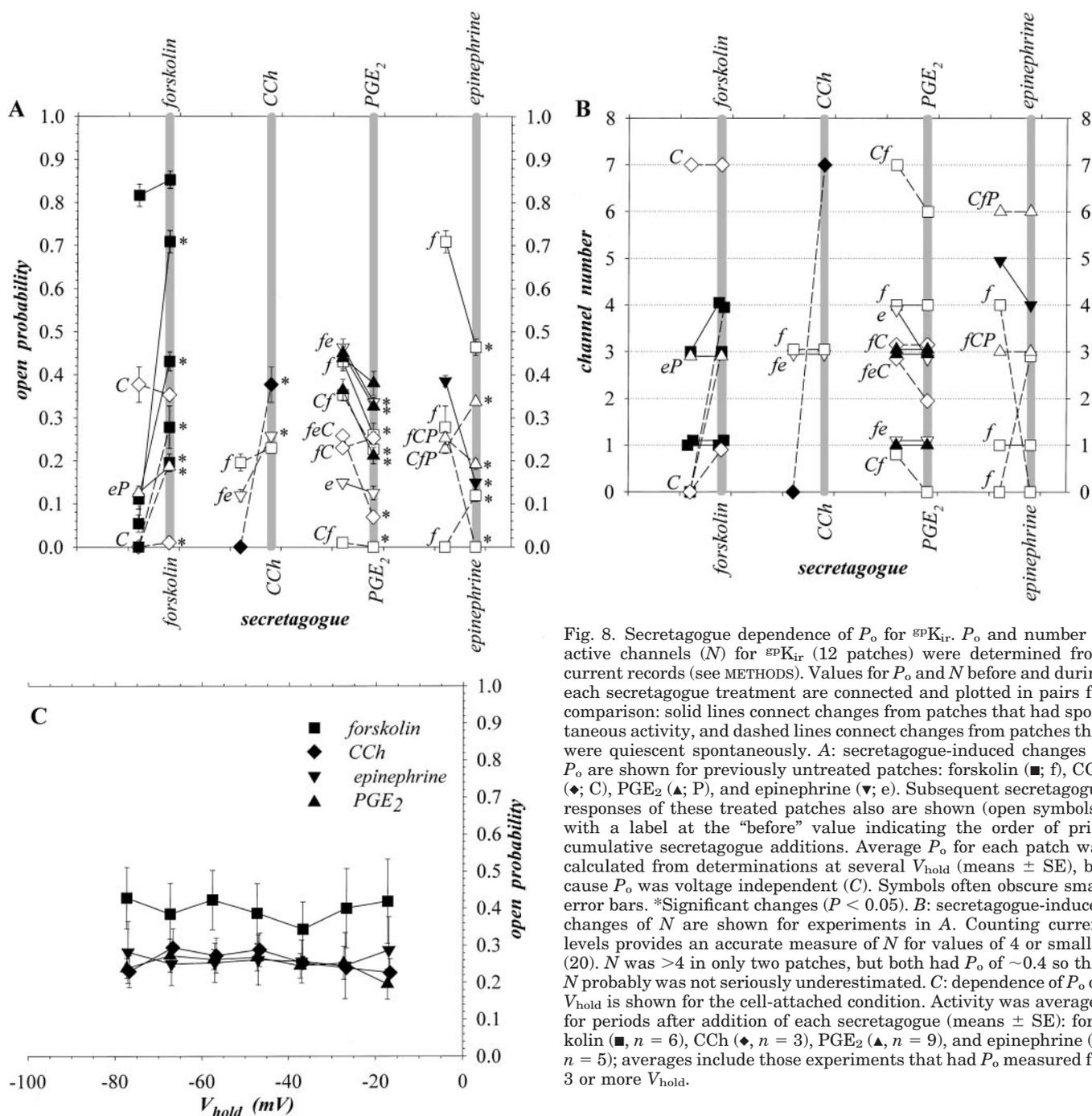
Fig. 8. Secretagogue dependence of P_o for $^{gp}K_{ir}$. P_o and number of active channels (N) for $^{gp}K_{ir}$ (12 patches) were determined from current records (see METHODS). Values for P_o and N before and during each secretagogue treatment are connected and plotted in pairs for comparison: solid lines connect changes from patches that had spontaneous activity, and dashed lines connect changes from patches that were quiescent spontaneously. A: secretagogue-induced changes of P_o are shown for previously untreated patches: forskolin (■; f), CCh (♦; C), PGE$_2$ (▲; P), and epinephrine (▼; e). Subsequent secretagogue responses of these treated patches also are shown (open symbols), with a label at the "before" value indicating the order of prior cumulative secretagogue additions. Average P_o for each patch was calculated from determinations at several V_{hold} (means ± SE), because P_o was voltage independent (C). Symbols often obscure small error bars. *Significant changes ($P < 0.05$). B: secretagogue-induced changes of N are shown for experiments in A. Counting current levels provides an accurate measure of N for values of 4 or smaller (20). N was >4 in only two patches, but both had P_o of ∼0.4 so that N probably was not seriously underestimated. C: dependence of P_o on V_{hold} is shown for the cell-attached condition. Activity was averaged for periods after addition of each secretagogue (means ± SE): forskolin (■, $n = 6$), CCh (♦, $n = 3$), PGE$_2$ (▲, $n = 9$), and epinephrine (▼, $n = 5$); averages include those experiments that had P_o measured for 3 or more V_{hold}.

three groups, C$_2$ through C$_4$. Most $^{gp}K_{ir}$ (8 of 10) had fitted components in both C$_2$ and C$_3$. Together, the simultaneous presence of the four shortest components suggests that these states were distinct and not variations within fewer states. In particular, the closely spaced groups C$_2$ and C$_3$ occurred in six successive 10-s intervals of the record in Fig. 9G (data not shown), indicating that the time constant for a single state was not simply drifting within this range unless the change oscillated continuously on a time scale much shorter than 10 s. Group C$_5$ appeared distinct because two $^{gp}K_{ir}$ were fit well with five components, C$_1$ through C$_5$,

and one other had both components C$_4$ and C$_5$. A group C$_6$ component was observed for two $^{gp}K_{ir}$ with low P_o, one in combination with C$_4$ and C$_5$. Thus, although secretagogue-induced changing of rates for entering and exiting a state could blur groupings of time constants, the minimum number of closed states for $^{gp}K_{ir}$ was five, but possibly six.

Burst analysis supported the presence of two open states. Bursts were delimited by closed durations longer than 1 ms. This duration was chosen to ignore most of the closures due to the shortest apparent closed state, C$_1$. All of the $^{gp}K_{ir}$ with spontaneous activity had

burst-duration histograms fit by two exponentials (Fig. 10A). Prolongation of the longer bursts in the low-P_o mode compared with the medium-P_o mode was consistent with the relative paucity of closures longer than 1 ms (Fig. 10B) such that burst termination is delayed substantially. Distributions of open durations during bursts were similar to all openings (data not shown). Presence of the brief burst mode (0.9–1.2 ms) during spontaneous low P_o activity (Fig. 10A) suggests that a low proportion of events (<5%) occurred in the short open state, O_S (Fig. 9A).

Excision led to increased P_o of $^{gp}K_{ir}$ similar to the medium-P_o spontaneous activity mode (Fig. 4). Open time constants for the excised condition (1.1 ± 0.2 ms, 24 ± 5%, and 3.5 ± 0.8 ms, 76 ± 5%, n = 3) were indistinguishable from those in the medium-P_o mode but significantly shorter (P < 0.05) than that for the low-P_o mode (Fig. 10A). The distribution of closures for the excised condition and medium-P_o mode differed from the low-P_o mode by a decreased proportion of events in C_1, an increase in C_2, and a lack of events in C_5 and C_6 (Fig. 10B). Excision appeared to have produced an increase in P_o by recreating the kinetic conditions of the spontaneous medium-P_o mode.

Reductions in P_o by epinephrine and PGE_2 after forskolin stimulation (Fig. 9, G and H) occurred with a roughly equal and relatively large proportion of closures in C_2 and C_3. For another $^{gp}K_{ir}$, PGE_2 reduced P_o from a spontaneous medium-P_o mode by decreasing the proportion of closures in C_2 and increasing the proportion in C_3 (data not shown) such that the final distribution was similar to that during forskolin/PGE_2 stimulation (Figs. 9H and 10B). Epinephrine and PGE_2 appeared to decrease P_o largely through a shift of closed events into C_2 and C_3 as well as a relative shift of open events into O_S.

Cytoplasmic regulators. Distinctions between known inwardly rectified K⁺ channels can be made, in part, from sensitivities to solution composition at the cytoplasmic face of the channel. Notably, dependence on Ca^{2+} and pH can be used to aid in distinguishing among intermediate-conductance Ca^{2+}-activated K⁺ channels (IK1; *KCNN4*), inward rectifier K⁺ channels (Kir; *KCNJ*), and so-called background K⁺ channels (TWIK; *KCNK1*) (10). Activity of $^{gp}K_{ir}$ was similar with bath pH of 7.2 and 6.6 (Fig. 11A), whereas increasing bath pH to 8.1 reduced $^{gp}K_{ir}$ activity modestly (n = 3). Because renal epithelial K⁺ channel (ROMK, Kir1.1; *KCNJ1*) activity decreases with acidification (9, 36), another channel type apparently was responsible for this $^{gp}K_{ir}$ observed in crypts. Reduction in bath solution free Ca^{2+} (Fig. 11B) did not lead to lower activity for $^{gp}K_{ir}$ (n = 4), indicating that IK1 (13, 23) alone could not be responsible for producing these currents.

DISCUSSION

Active ion secretion across epithelia produces an osmotic gradient that drives fluid secretion (14, 15). The lumen negative transepithelial electrical potential difference produced by Cl⁻ secretion results from a cellular mechanism employing apical membrane Cl⁻ channels and basolateral membrane K⁺ channels. Together with the K⁺ concentration gradient developed by operation of the Na^+-K^+ pump, basolateral membrane K⁺ conductance serves to generate a cell negative basolateral membrane electrical potential difference (V_b). Apical membrane Cl⁻ channels allow Cl⁻ exit into the lumen, driven by the electrochemical gradient. This gradient is directed outward because of the influence of basolateral membrane K⁺ channels on apical membrane electrical potential difference (V_a). Continued Cl⁻ secretion, and thus fluid secretion, depends on a basolateral membrane K⁺ conductance large enough to maintain Cl⁻ exit across the apical membrane by ensuring that V_a exceeds the size of the inwardly directed concentration gradient.

Colonic Cl⁻ secretion in mammals is accompanied by electrogenic K⁺ secretion, apparently by inclusion of apical membrane K⁺ channels in Cl⁻ secretory cells (15, 41). For colonic secretory cells, therefore, K⁺ channels in both apical and basolateral membranes contribute to maintaining a cell negative V_a that promotes Cl⁻ secretion. In addition, K⁺ conductance of apical membrane relative to basolateral membrane contributes to determining the proportion of intracellular K⁺ exiting into the lumen. Elevated luminal K⁺ concentration (19) would lower the K⁺ concentration gradient across the apical membrane and thereby reduce the ability of apical K⁺ channels to ensure conductive Cl⁻ exit. Relative rates of Cl⁻ and K⁺ secretion vary among mammalian species (15), but in guinea pig distal colon these electrogenic flows are roughly equal when stimulated by high concentrations (>100 nM) of PGE_2 (17, 41). Activation by epinephrine (15, 41) or low concentrations (<100 nM) of PGE_2 (17, 41) produces electrogenic K⁺ secretion without accompanying Cl⁻ secretion. Cl⁻ entering via basolateral membrane Na^+-K^+-$2Cl^-$ cotransporters during this type of sustained electrogenic K⁺ secretion apparently exits across the basolateral membrane through Cl⁻ channels (15, 30, 41). Control of basolateral K⁺ channels during primary electrogenic K⁺ secretion, thus, also would contribute to maintaining a driving force for Cl⁻ exit from the cell as well as to determining the proportion of K⁺ exiting into the lumen.

K⁺ channel types. Several classes of K⁺ channels have been identified by amino acid sequence homology (10, 27). Although all seem to conserve a general pore-forming component, wide variation occurs in other portions of the sequence that presumably control channel activation and kinetic behavior. Three of these K⁺ channel types exhibit distinct inwardly rectified γ: Kir (*KCNJ*), IK1 (*KCNN4*), and TWIK (*KCNK1*) (10). With symmetrical 150 mM K⁺ concentration, γ at V_m = 0 mV is 30, 16, and 28 pS for Kir1.1 (9), IK1 (23, 25), and TWIK (29), respectively. Specific sensitivities to pH, Ca^{2+}, and ATP also contribute to a functional identification of these channel types (10). In particular, the ROMK channel (Kir1.1; *KCNJ1*) is inhibited by acidification at the cytoplasmic side of the channel (9, 36). Increasing cytoplasmic ATP also inactivates ROMK
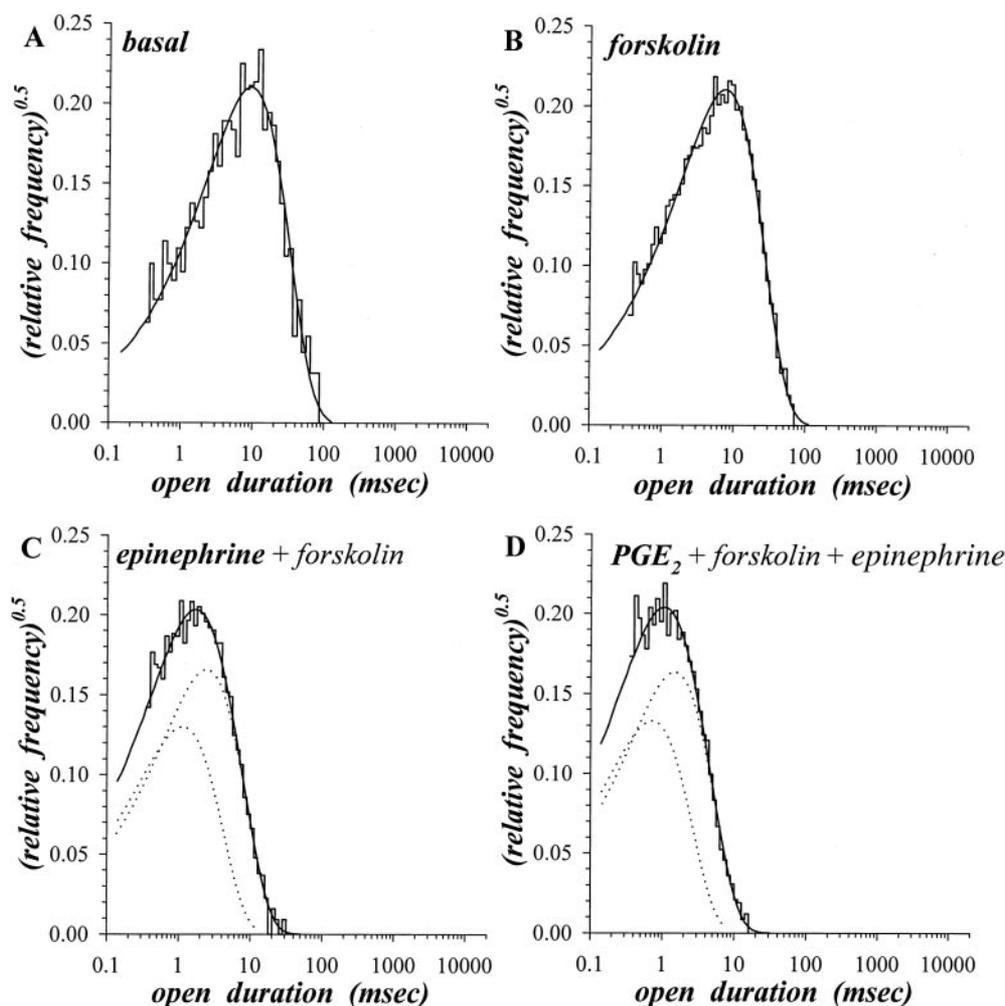
Fig. 9. Secretagogue dependence of kinetics for $^{gp}K_{ir}$. Histograms of open (*A–D*) and closed durations (*E–H*) are shown in which log binning was used (see METHODS) for a single $^{gp}K_{ir}$ during cumulative addition of several secretagogues while cell-attached (see Fig. 7*B*). V_{hold} was −70 mV. Each current record was ~50 s in length with a various number of events in each condition: basal (740), forskolin (5,479), epinephrine (8,252), and PGE₂ (8,380). Open-duration histograms for basal and forskolin conditions had a peak fit well by a single exponential; open-duration histograms for epinephrine and PGE₂ conditions had a peak fit best by a mixture of 2 exponentials. Relative frequency was obtained by normalizing to the number of open events, estimated from the fitted exponentials. Individual fit components are shown as dotted lines. Fitted open time constants and proportions of events (in parentheses) were basal, 9.4 ms; forskolin, 7.7 ms; epinephrine, 1.1 ms (0.38) and 2.4 ms (0.62); and PGE₂, 0.7 ms (0.40) and 1.5 ms (0.60). Closed-duration histograms exhibited multiple peaks requiring a mixture of exponentials for an adequate fit; relative frequency was obtained by normalizing to the number of open events for that condition. Fitted closed time constants and proportions of events (in parentheses) were basal, 0.3 ms (0.94), 8.6 ms (0.03), 187 ms (0.02), and 14.5 s (0.01); forskolin, 0.3 ms (0.87), 3.7 ms (0.06), 10.8 ms (0.06), and 101 ms (0.01); epinephrine, 0.3 ms (0.45), 2.3 ms (0.30), 6.6 ms (0.24), and 59.3 ms (0.01); and PGE₂, 0.3 ms (0.54), 3.4 ms (0.30), 8.3 ms (0.14), and 50.4 ms (0.01). Kinetic parameters from currents at V_{hold} of −80 mV were similar.

(Kir1.1; *KCNJ1*) (9, 36); association with a regulatory subunit, the sulfonylurea receptor, confers even greater ATP sensitivity to Kir6 (10). Activation by cytoplasmic Ca^{2+} is a key feature of IK1 shared with BK (slo; *KCNMA*) (10). The TWIK channel has been termed a background channel because it does not have any direct dependence on pH, Ca^{2+}, or V_m (10, 29). Behavior of K⁺ channels in native circumstances may vary from characteristics of overexpressed versions, however, because K⁺ channels may exist as heteromultimeric assemblies of channel and regulatory subunits that result in divergent properties (10, 27, 43, 51).

Colonic K⁺ channels. Three major types of K⁺ channels have been observed in cell-attached patches on basolateral membrane of colonic and small intestinal crypts (55): large-conductance K⁺ channels (5, 6, 26, 32, 33, 35, 42), intermediate-conductance Ca^{2+}-activated K⁺ channels (4, 5, 20, 35, 42, 44), and very small conductance K⁺ channels (57). Nonselective cation channels, with γ of 20–40 pS, also have been observed in basolateral membranes of colonic epithelial cells (4, 6, 42, 47), similar in size to those observed in guinea pig crypts. Large-conductance K⁺ channels in crypts have γ ranging from ~100 pS to >200 pS, and some are
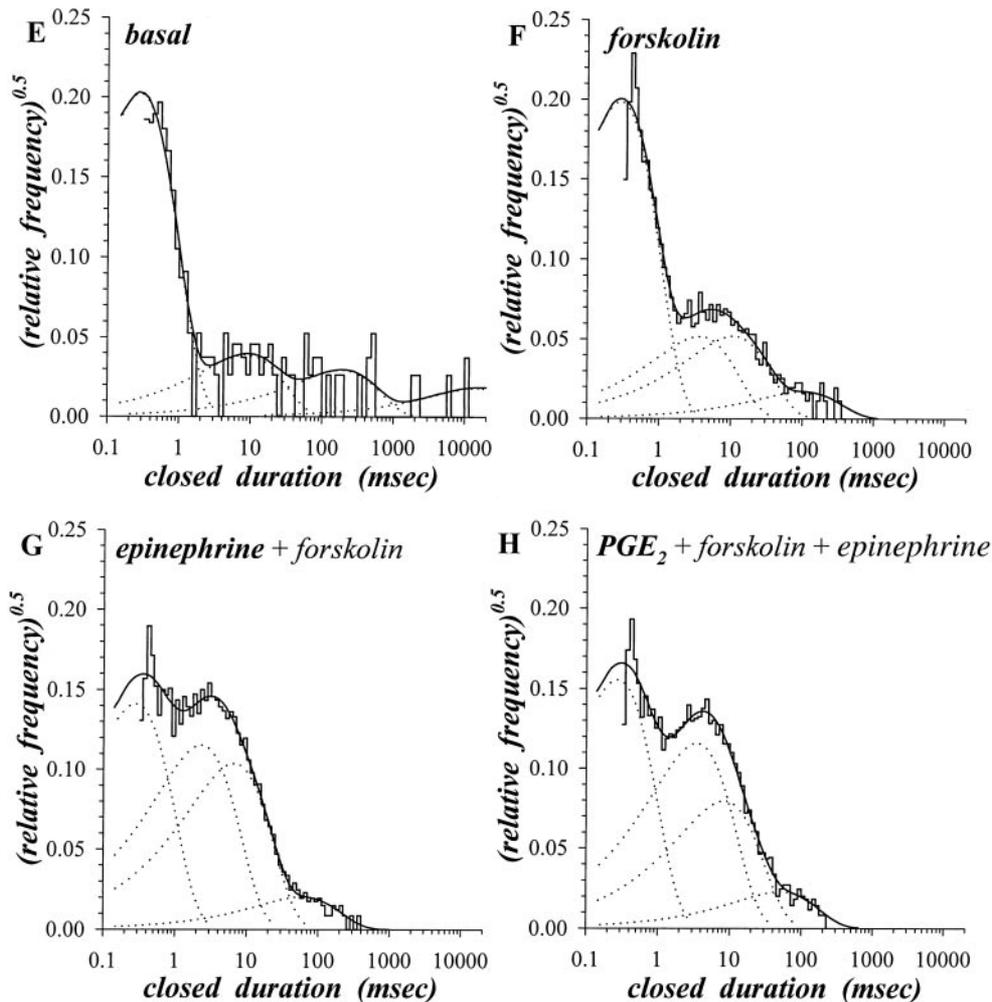
Fig. 9—*Continued*

activated by increases in Ca^{2+} activity at the cytoplasmic face of the channel (5, 26, 32, 33, 35). Kinetic behavior and large conductance suggest that these K$^+$ channels, and those observed in guinea pig crypts (Figs. 1*D* and 2), are intestinal assemblies of the BK (slo; *KCNMA*) channel (*10*). Colonic intermediate-conductance Ca^{2+}-activated K$^+$ channels often are inwardly rectified (5, 20, 39, 42) with γ of 30–35 pS in symmetrical 150 mM K$^+$ concentrations at $V_m = 0$ mV. Inwardly rectified Ca^{2+}-activated K$^+$ channels with γ of ~20 pS have been observed as well in the colonic tumor cell line T84 (11, 49). Identification of these K$^+$ channels as IK1 (*KCNN4*) (*10*) is supported further by detection of mRNA for IK1 in T84 cells and colonic epithelial cells (56). Another K$^+$ channel with very small conductance (<4 pS) also has been detected in colonic crypts, with the use of noise analysis (57), similar in size to KvLQT1 (*KCNQ1*) assembled with the regulatory subunit minK$^+$ (*KCNE*) (58). Identity of this crypt K$^+$ channel as KvLQT1/minK$^+$ (*KCNQ1/KCNE*) is supported by in situ hybridization localizing mRNA for both subunits in colonic crypt cells (46).

The predominant K$^+$ channel type found in this study of guinea pig distal colonic crypts was an inwardly rectified K$^+$ channel, ^{gp}K$_{ir}$ (Fig. 1*B*). A larger conductance K$^+$ channel was observed rarely (Fig. 1*D*) that may correspond to the BK channel (slo; *KCNMA*) (10). Identity of the ^{gp}K$_{ir}$ observed in basolateral membranes is uncertain. With physiological external K$^+$ and Na$^+$ concentrations (Figs. 1*A* and 2), ^{gp}K$_{ir}$ apparently had a linear current-voltage relation. A less commonly observed inwardly rectified K$^+$ channel (Fig. 1*C*), which may be another conductance state of ^{gp}K$_{ir}$, had steeper rectification than ^{gp}K$_{ir}$ at negative V_m (Fig. 3*E*). Insensitivity to changes in Ca^{2+} activity on the cytoplasmic side of ^{gp}K$_{ir}$ (Fig. 10*B*) suggests that IK1 (*KCNN4*) (10) is not a candidate protein unless other associating components could modify Ca^{2+} dependence. Insensitivity to acid pH (Fig. 10*A*) suggests that ROMK (Kir1.1; *KCNJ1*) (9, 36) also is not the protein forming ^{gp}K$_{ir}$. The lack of these specific controlling factors for ^{gp}K$_{ir}$ suggests TWIK (*KCNK1*) (10) as a possibility, but γ for TWIK with symmetrical 150 mM K$^+$ concentrations (at $V_m = 0$ mV) is approximately twofold larger (29) than for ^{gp}K$_{ir}$ (Figs. 3*B*). Thus ^{gp}K$_{ir}$ does not conform easily to any of these known inwardly rectified K$^+$ channel types.
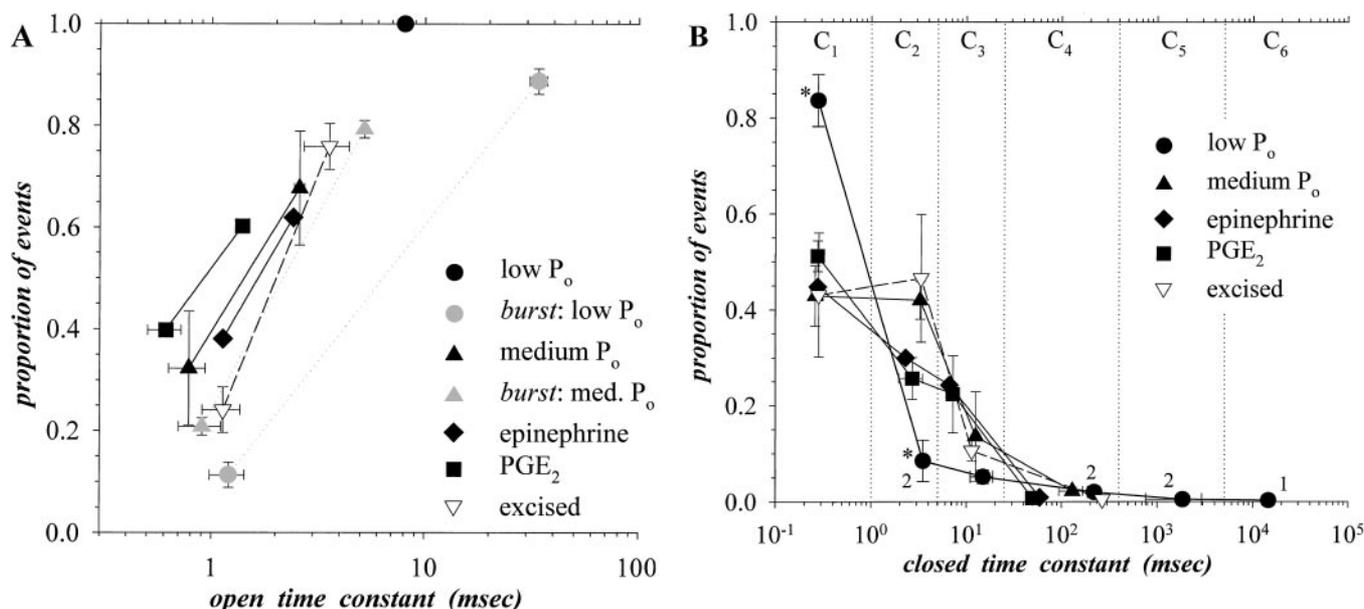
Fig. 10. Open and closed states of $^{gp}K_{ir}$. Time constants and proportions of events for kinetic states obtained from fits of duration histograms to mixtures of exponentials were averaged from patches containing only 1 $^{gp}K_{ir}$ (means $\pm$ SE, range is shown for $n = 2$). Spontaneous cell-attached activity with low P_o ($n = 3$) and medium P_o ($n = 3$) together with excised I/O activity ($n = 3$) are shown. Activity during PGE_2 ($n = 2$) and epinephrine ($n = 1$) treatments also is shown. A: open states of shorter (O_S) and longer (O_L) time constants are connected for each condition. Burst analysis (1-ms delimiter) yielded burst-duration histograms fit by a mixture of 2 exponentials. B: closed time constants clustered into groups. For those $^{gp}K_{ir}$ that did not exhibit a fit in a particular closed-duration group, a proportion of zero was included in the group average; n is indicated on plots for those cases. *Significantly different from medium-P_o or excised conditions ($P < 0.05$). Vertical dotted lines demarcate apparent ranges of observed time constants; average values (from spontaneous activity) for each group were C_1, 0.3 ± 0.01 ms, $n = 10$; C_2, 3.2 ± 0.1 ms, $n = 9$; C_3, 12.7 ± 1.5 ms, $n = 8$; C_4, 148.4 ± 35.2 ms, $n = 8$; C_5, 1.31 ± 54 s, $n = 4$; and C_6, 25.2 ± 10.7 s, $n = 2$.

Conduction (Fig. 3E) and activation (Fig. 11) properties for $^{gp}K_{ir}$ suggest that guinea pig colonic crypts exhibit a K+ channel distinct from those already characterized in basolateral membranes for this type of epithelial cell (55). However, several commonalties can be found between $^{gp}K_{ir}$ and previously observed intermediate-conductance K+ channels. ROMK has a subconductance state of ~13 pS corresponding to a particular phosphorylated state (34). Coexpression of the Cl⁻ channel cystic fibrosis transmembrane conductance
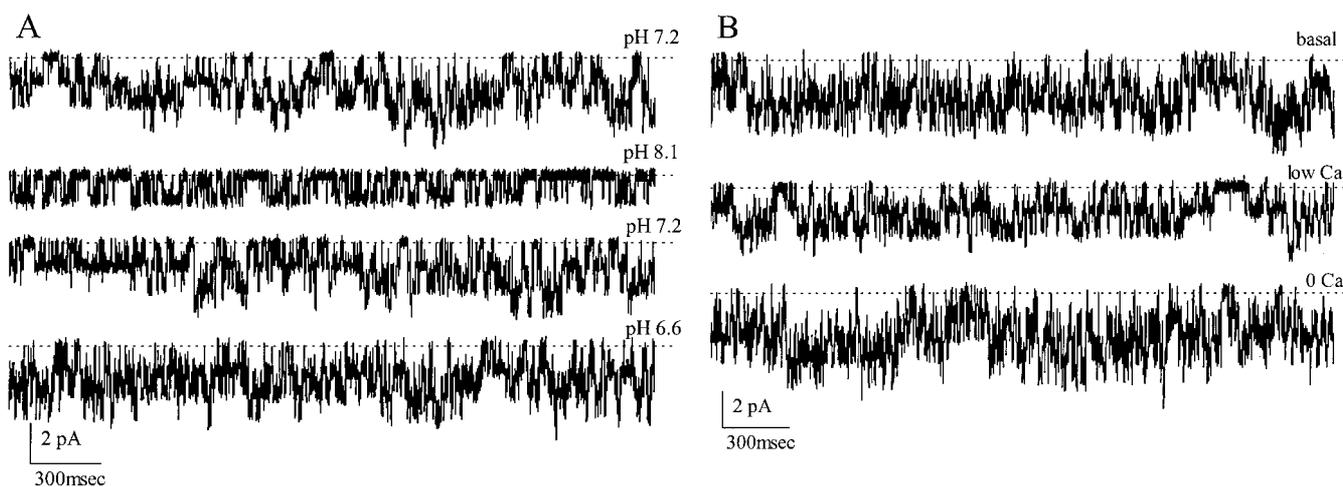

Fig. 11. Control of $^{gp}K_{ir}$. Currents from $^{gp}K_{ir}$ were recorded in excised I/O configuration during changes in bath solution. Pipette solution was high-K+. Closed states are indicated by dashed lines. A: currents are shown for bath solution pH (see methods) of 7.2, 8.1, or 6.6 for V_{hold} of −50 mV. P_o was voltage independent: 0.39 ± 0.02 (pH 7.2), 0.39 ± 0.03 (pH 6.6), and 0.28 ± 0.03 (pH 8.1); the number of active $^{gp}K_{ir}$ was 4. B: currents are shown for bath solution free Ca^{2+} concentration (see METHODS) of ~10 μM (basal), ~100 nM (low Ca^{2+}), or <10 nM (0 Ca^{2+}) for V_{hold} of −50 mV. P_o was voltage independent: 0.46 ± 0.01 (basal), 0.45 ± 0.01 (low Ca^{2+}), and 0.42 ± 0.01 (0 Ca^{2+}); the number of active $^{gp}K_{ir}$ was 5.

regulator with ROMK leads to inwardly rectified K$^+$ channels with γ of about half ($\sim$15 pS) that for ROMK alone (43). In addition, heteromeric assembly of Kir4.1 with Kir5.1 increases γ by approximately twofold (51). Ca^{2+}-dependent K$^+$ channels in T84 cells have low P_o independent of V_m (50), similar to that for ^{gp}K$_{ir}$ (Fig. 4A). Other Ca^{2+}-dependent K$^+$ channels of intermediate conductance exhibit P_o that increases (5) or decreases (56) at more positive V_m. ROMK has high P_o ($\sim$0.9) that is relatively independent of V_m (40). High relative permeability to Rb$^+$ (Fig. 3) appears to distinguish ^{gp}K$_{ir}$ from both ROMK (8) and IK1 (49). Although none of the currently established K$^+$ channels (10) has identical characteristics to ^{gp}K$_{ir}$, a distinct assembly of channel and regulatory subunits (27) presumably confers the properties observed for ^{gp}K$_{ir}$.

Regulation of Cl$^-$ and K$^+$ secretion. Control of ^{gp}K$_{ir}$ in the basolateral membrane participates in production of Cl$^-$ and K$^+$ secretion by contributing to maintenance of V_a that drives Cl$^-$ exit into the lumen while also adjusting the proportion of K$^+$ exit into the lumen. Activation of ^{gp}K$_{ir}$ occurred with two Cl$^-$ secretagogues, forskolin and CCh (Figs. 5–7), consistent with this channel being used to augment basolateral membrane K$^+$ conductance. Both the number of active ^{gp}K$_{ir}$ (N_K) and P_o increased (Fig. 8) such that basolateral membrane K$^+$ conductance (g^K) would increase: $g^K = N_K P_o \gamma^K$. The K$^+$ secretagogues PGE$_2$ and epinephrine led to decreased g^K primarily by reducing P_o (Fig. 8) and occasionally by deactivating ^{gp}K$_{ir}$ (N_K). This type of control would suit the requirements of balancing K$^+$ and Cl$^-$ secretory rates by moderating basolateral membrane K$^+$ conductance within a precise range.

Regulatory modes for ^{gp}K$_{ir}$ can be distinguished on the basis of the kinetics producing P_o. Spontaneous activity exhibited two modes, with low and moderate P_o (Figs. 4A and 10). The cAMP-dependent agent forskolin produced moderate P_o with kinetics different from the spontaneous mode (Figs. 8A, 9, and 10). The K$^+$ secretagogues PGE$_2$ and epinephrine reduced P_o to an intermediate level with kinetics distinguishable from the other three modes (Figs. 8A, 9, and 10). These four kinetic modes of ^{gp}K$_{ir}$ presumably are produced by distinct regulatory mechanisms characteristic of the components making up this channel complex.

A kinetic scheme for ^{gp}K$_{ir}$ must include two open states and at least five, possibly six, closed states (Fig. 10). Although the connections for these states were not determined uniquely by the data available, several features controlling each mode were apparent. Long-duration closures in the C$_5$ and C$_6$ groups were associated only with the low-P_o mode. The medium-P_o mode also differed from the low-P_o mode by having similar contributions from C$_1$ and C$_2$. Intermediate P_o of the K$^+$ secretory mode occurred with a relatively high contribution from C$_3$. Both the low-P_o and forskolin modes had open durations dominated by a single state with a time constant approximately four times longer than O$_L$ of the medium-P_o and K$^+$ secretory modes.

A common feature of many K$^+$ channels, including ^{gp}K$_{ir}$, appears to be activation through reduced number of long-duration closures, although the mechanism producing this kinetic change is distinct for each channel type. Similar to the loss with forskolin of ^{gp}K$_{ir}$ closed durations ranging from 0.4 to 10 s (Fig. 9, E and F), cAMP-dependent activation eliminated longer closed durations of an ATP-dependent, inwardly rectified K$^+$ channel in the basolateral membrane of proximal tubules (37). Protein kinase A (PKA) together with ATP stimulates an 85-pS K$^+$ channel from the lateral membrane of cortical collecting duct largely through a decreased number of the long-duration closures as well as an increased number of the long-duration openings (53). Modulation of ROMK (Kir1.1; *KCNJ1*) via alkalinization increases P_o by decreasing the number of long-duration closures without changing open durations (9, 36). Heteromeric Kir4.1-Kir5.1 (*KCNJ10–KCNJ16*) also increases P_o upon alkalinization through a loss of long-duration closures (59). Stimulation of IK1 (*KCNN4*) by the K$^+$ channel opener 1-EBIO occurs through a decrease in long closed durations without any change in open durations (48). A small-conductance Ca^{2+}-activated K$^+$ channel (SK2; *KCNN2*) activates with increased cytoplasmic Ca^{2+}, in part, by losing long duration closures (21).

Activation of K$^+$ channels can result from phosphorylation via cellular kinases (54). Both the cAMP-dependent PKA and the Ca^{2+}-dependent protein kinase C (PKC) have been implicated in K$^+$ channel regulation (10, 27, 54). Increasing cAMP either directly or with forskolin stimulates activity of BK channels in rabbit colonic crypts (33), intermediate-conductance K$^+$ channels (IK1) in human colonic crypts (44), and very small conductance K$^+$ channels (KvLQT1/minK) in rat colonic crypts (57). Loss of channel activity after excision into an I/O configuration often can be returned by adding ATP to the bathing solution or by inhibiting phosphatase activity (2), suggesting that channel P_o can be controlled through a balance between kinase and phosphatase activity (13, 28, 39, 50, 54, 57).

The tendency for excision to increase P_o of ^{gp}K$_{ir}$ (Fig. 4) suggests that a cytoplasmic inhibitory component was lost. One possibility could be that a membrane-resident phosphatase (2) dephosphorylated ^{gp}K$_{ir}$ at an inhibitory site, similar to the negative influence of PKC on ROMK (54). Excision activation (Fig. 4B) and forskolin activation (Figs. 6A and 7B) both increase P_o of ^{gp}K$_{ir}$ into the range of the spontaneous medium-P_o mode (Fig. 4A). In part, P_o increased because ^{gp}K$_{ir}$ did not enter long-lived closed states. However, during forskolin treatment ^{gp}K$_{ir}$ openings were predominately to the longer open state (Fig. 9B), whereas after excision openings occurring to both states and O$_L$ had a shorter time constant (Fig. 10A). These two modes of activation could be reconciled with a phosphorylation/dephosphorylation mechanism if at least two phosphorylation sites were to exist with opposing action on P_o such that relieving the negative control is sufficient for increased activity.

Cholinergic activation of ^{gp}K$_{ir}$ apparently does not proceed through direct influence of cytoplasmic Ca^{2+} on the channel (Fig. 10B), as occurs for other interme-

diate-conductance K$^+$ channels (4, 11, 13, 23, 44, 49). Instead, Ca^{2+} dependence may be indirect, conferred perhaps via a Ca^{2+}-activated kinase such as PKC or calmodulin-dependent kinase. Reduction of ^{gp}K$_{ir}$ P_o by the K$^+$ secretagogues PGE$_2$ and epinephrine (Fig. 8) generally did not drop to the low spontaneous levels (Fig. 4A). Rather than returning to a condition with long-duration closures, closures to states with intermediate time constants increased in number (Figs. 9 and 10). Somatostatin also reduces P_o to a non-zero value for a cAMP-activated K$^+$ channel in human colonic crypts in concert with only a ~14% decrease of intracellular cAMP levels (45). Although PGE$_2$ and epinephrine can act through receptors that increase cytoplasmic cAMP (15), this inhibitory control of ^{gp}K$_{ir}$ may occur through another second messenger pathway such that several separable mechanisms may be involved in controlling ^{gp}K$_{ir}$ kinetics.

Colonic crypts possess several types of K$^+$ channels (55), and each may serve specific facets of the cellular requirements for K$^+$ conductance. These needs may not be identical for the two predominant cell types in the crypt, columnar and goblet. Because mucus release from columnar cells and goblet cells is controlled by distinct secretagogues (16), responsiveness to cholinergic stimulation by CCh may indicate a goblet cell regulatory mode. However, attempts to examine cell type-specific responses may have been complicated by differences in patching efficacy. Also in this study, incidences of channel appearance and activation were low enough to obscure further any cell type distinctions that might exist. However, the contribution of ^{gp}K$_{ir}$ to basolateral membrane K$^+$ conductance of crypt epithelium would be a 9-pS channel (Fig. 2) with a P_o that can be modulated in the range from 0.1 to 0.5 (Fig. 8). For the situations of Cl$^-$ and K$^+$ secretion, this feature of subtle modulations in P_o may allow secretory cells to adjust basolateral K$^+$ conductance for a precise balance in rates of K$^+$ exit and maintenance of membrane electrical potential differences (V_a and V_b).

REFERENCES

1. **Barry PH and Lynch JW.** Liquid junction potentials and small cell effects in patch-clamp analysis. *J Membr Biol* 121: 101–117, 1991.
2. **Becq F.** Ionic channels rundown in excised membrane patches. *Biochim Biophys Acta* 1286: 53–63, 1996.
3. **Bjerknes M and Cheng H.** Methods for the isolation of intact epithelium from the mouse intestine. *Anat Rec* 199: 565–574, 1981.
4. **Bleich M, Riedemann N, Warth R, Kerstan D, Leipziger J, Hör M, Van Driessche W, and Greger R.** Ca^{2+} regulated K$^+$ and non-selective cation channels in the basolateral membrane of rat colonic crypt base cells. *Pflügers Arch* 432: 1011–1022, 1996.
5. **Burckhardt B and Gögelein H.** Small and maxi K$^+$ channels in the basolateral membrane of isolated crypts from rat distal colon: single-channel and slow whole-cell recordings. *Pflügers Arch* 420: 54–60, 1992.
6. **Butt AG and Hamilton KL.** Ion channels in isolated mouse jejunal crypts. *Pflügers Arch* 435: 528–538, 1998.
7. **Chang EB and Rao MC.** Intestinal water and electrolyte transport: mechanisms of physiological and adaptive responses. *Physiology of the Gastrointestinal Tract*, edited by Johnson LR. New York: Raven, 1994, p. 2027–2081.
8. **Chepilko S, Zhou H, Sackin H, and Palmer LG.** Permeation and gating properties of a cloned renal K$^+$ channel. *Am J Physiol Cell Physiol* 268: C389–C401, 1995.
9. **Choe H, Zhou H, Palmer LG, and Sackin H.** A conserved cytoplasmic region of ROMK modulates pH sensitivity, conductance and gating. *Am J Physiol Renal Physiol* 273: F516–F529, 1997.
10. **Coetzee WA, Amarillo Y, Chiu J, Chow A, Lau D, McCormack T, Moreno H, Nadal MS, Ozaita A, Pountney D, Saganich M, Vega-Saenz de Miera, E, and Rudy B.** Molecular diversity of K$^+$ channels. *Ann NY Acad Sci* 868: 233–285, 1999.
11. **Devor DC and Frizzell RA.** Calcium-mediated agonists activate an inwardly rectified K$^+$ channel in colonic secretory cells. *Am J Physiol Cell Physiol* 265: C1271–C1280, 1993.
12. **Dwyer TM.** A patch clamp primer. *J Electrophysiol Tech* 12: 15–29, 1985.
13. **Gerlach AC, Gangopadhyay NN, and Devor DC.** Kinase-dependent regulation of the intermediate conductance, calcium-dependent K channel, hIK1. *J Biol Chem* 275: 585–598, 2000.
14. **Halm DR and Frizzell RA.** Intestinal chloride secretion. *Textbook of Secretory Diarrhea*, edited by Lebenthal E and Duffey M. New York: Raven, 1990, p. 47–58.
15. **Halm DR and Frizzell RA.** Ion transport across the large intestine. *Handbook of Physiology. Intestinal Absorption and Secretion.* Bethesda, MD: Am. Physiol. Soc., 1991, vol. IV, p. 257–274.
16. **Halm DR and Halm ST.** Secretagogue response of goblet cells and columnar cells in human colonic crypts. *Am J Physiol Cell Physiol* 277: C501–C522, 1999. [Corrigenda. *Am J Physiol Cell Physiol* 278: January 2000, following table of contents.]
17. **Halm DR and Halm ST.** Prostanoids stimulate K secretion and Cl secretion in guinea pig distal colon via distinct pathways. *Am J Physiol Gastrointest Liver Physiol* 281: G984–G996, 2001.
18. **Halm DR, Kirk KL, and Sathiakumar KC.** Stimulation of Cl permeability in colonic crypts of Lieberkühn measured with a fluorescent indicator. *Am J Physiol Gastrointest Liver Physiol* 265: G423–G431, 1993.
19. **Halm DR and Rick R.** Secretion of K and Cl across colonic epithelium: cellular localization using electron microprobe analysis. *Am J Physiol Cell Physiol* 262: C1392–C1402, 1992.
20. **Hamilton KL and Butt AG.** 1-EBIO stimulates Cl$^-$ secretion by activating a basolateral K$^+$ channel in the mouse jejunum. *Pflügers Arch* 439: 158–166, 1999.
21. **Hirschberg B, Maylie J, Adelman JP, and Marrion NV.** Gating of recombinant small-conductance Ca-activated K$^+$ channels by calcium. *J Gen Physiol* 111: 565–581, 1998.
22. **Horn R.** Estimating the number of channels in patch recordings. *Biophys J* 60: 433–439, 1991.
23. **Ishi TM, Silva C, Hirschberg B, Bond CT, Adelman JP, and Maylie J.** A human intermediate conductance calcium-activated potassium channel. *Proc Natl Acad Sci USA* 94: 11651–11656, 1997.
24. **Jackson MB.** Stationary single-channel analysis. *Methods Enzymol* 207: 729–746, 1992.
25. **Jensen BS, Strøbæk D, Christophersen P, Jørgensen TD, Hansen C, Silahtaroglu A, Olesen S, and Ahring PK.** Characterization of the cloned human intermediate-conductance Ca^{2+}-activated K$^+$ channel. *Am J Physiol Cell Physiol* 275: C848–C856, 1998.
26. **Klærke DA, Wiener H, Zeuthen T, and Jørgensen PL.** Ca^{2+} activation and pH dependence of a maxi K$^+$ channel from rabbit distal colon epithelium. *J Membr Biol* 136: 9–21, 1993.
27. **Kubo Y.** Overview of K channel families: molecular bases of the functional diversity. *Handbook of Experimental Pharmacology. Pharmacology of Ionic Channel Function: Activators and Inhibitors*, edited by Endo M, Kurachi Y, and Mishina M. Berlin: Springer, 2000, vol. 147, p.157–176.
28. **Kubokawa M, McNicholas CM, Higgins MA, Wang W, and Giebisch G.** Regulation of ATP-sensitive K$^+$ channel by mem-

brane-bound protein phosphatases in rat principal tubule cell. *Am J Physiol Renal Fluid Electrolyte Physiol* 269: F355–F362, 1995.

29. **Lesage F, Guillemare E, Fink M, Duprat F, Lazdunski M, Romey G, and Barhanin J.** TWIK-1, a ubiquitous human weakly inward rectifying K⁺ channel with a novel structure. *EMBO J* 15: 1004–1011, 1996.

30. **Li Y and Halm DR.** Ion channels in epithelial cells of isolated crypts from guinea pig distal colon. *FASEB J* 14: A112, 2000.

31. **Lohrmann E and Greger R.** The effect of secretagogues on ion conductance of in vitro perfused, isolated rabbit colonic crypts. *Pflügers Arch* 427: 494–502, 1995.

32. **Lomax RB, Warhurst G, and Sandle GI.** Characteristics of two basolateral potassium channel populations in human colonic crypts. *Gut* 38: 243–247, 1996.

33. **Loo DDF and Kaunitz JD.** Ca²⁺ and cAMP activate K⁺ channels in the basolateral membrane of crypt cells isolated from rabbit distal colon. *J Membr Biol* 110: 19–28, 1989.

34. **MacGregor GG, Xu JZ, McNicholas CM, Giebisch G, and Hebert SC.** Partially active channels produced by PKA site mutation of the cloned renal K⁺ channel, ROMK2 (Kir1.1b). *Am J Physiol Renal Physiol* 275: F415–F422, 1998.

35. **McNicholas CM, Fraser G, and Sandle GI.** Properties and regulation of basolateral K⁺ channels in rat duodenal crypts. *J Physiol (Lond)* 477: 381–392, 1994.

36. **McNicholas CM, MacGregor GG, Islas LD, Yang Y, Hebert SC, and Giebisch G.** pH-dependent modulation of the cloned renal K⁺ channel, ROMK. *Am J Physiol Renal Physiol* 275: F972–F981, 1998.

37. **Mauerer UR, Boulpaep EL, and Segal AS.** Regulation of an inwardly rectifying ATP-sensitive K⁺ channel in the basolateral membrane of renal proximal tubule. *J Gen Physiol* 111: 161–180, 1998.

38. **Neher E.** Correction for liquid junction potential in patch clamp experiments. *Methods Enzymol* 207: 123–131, 1992.

39. **Nielsen MS, Warth R, Bleich M, Weyand B, and Greger R.** The basolateral Ca²⁺-dependent K⁺ channel in rat colonic crypt cells. *Pflügers Arch* 435: 267–272, 1998.

40. **Palmer LG, Choe H, and Frindt G.** Is the secretory K channel in the rat CCT ROMK? *Am J Physiol Renal Physiol* 273: F404–F410, 1997.

41. **Rechkemmer GR, Frizzell RA, and Halm DR.** Active potassium transport across guinea pig distal colon: action of secretagogues. *J Physiol (Lond)* 493: 485–502, 1996.

42. **Richards NW and Dawson DC.** Selective block of specific K⁺-conducting channels by diphenylamine-2-carboxylate in turtle colon epithelial cells. *J Physiol (Lond)* 462: 715–734, 1993.

43. **Ruknudin A, Schulze DH, Sullivan SK, and Welling PA.** Novel subunit composition of a renal epithelial K_ATP channel. *J Biol Chem* 273: 14165–14171, 1998.

44. **Sandle GI, McNicholas CM, and Lomax RB.** Potassium channels in colonic crypts. *Lancet* 343: 23–25, 1994.

45. **Sandle GI, Warhurst G, Butterfield I, Higgs NB, and Lomax RD.** Somatostatin peptides inhibit basolateral potassium channels in human colonic crypts. *Am J Physiol Gastrointest Liver Physiol* 277: G967–G975, 1999.

46. **Schroeder BC, Waldegger S, Fehr S, Bleich M, Warth R, Greger R, and Jentsch TJ.** A constitutively open potassium channel formed by KCNQ1 and KCNE3. *Nature* 403: 196–199, 2000.

47. **Siemer C, and Gögelein H.** Activation of nonselective cation channels in the basolateral membrane of rat distal colon crypt cells by prostaglandin E₂. *Pflügers Arch* 420: 319–328, 1992.

48. **Syme CA, Gerlach AC, Singh AK, and Devor DC.** Pharmacological activation of cloned intermediate- and small-conductance Ca²⁺-activated K⁺ channels. *Am J Physiol Cell Physiol* 278: C570–C581, 2000.

49. **Tabcharani JA, Harris RA, Boucher A, Eng JWL, and Hanrahan JW.** Basolateral K channel activated by carbachol in the epithelial cell line T84. *J Membr Biol* 142: 241–254, 1994.

50. **Tabcharani JA, Harris RA, Boucher A, Eng JWL, and Hanrahan JW.** Regulation of an inwardly rectifying K channel in the T84 epithelial cell line by calcium, nucleotides and kinases. *J Membr Biol* 142: 255–266, 1994.

51. **Tanemoto M, Kittaka N, Inanobe A, and Kurachi Y.** In vivo formation of a proton-sensitive K⁺ channel by heteromeric subunit assembly of Kir5.1 with Kir4.1. *J Physiol (Lond)* 525: 587–592, 2000.

52. **Teulon J.** Ca²⁺-activated nonselective cation channels. *Handbook of Experimental Pharmacology. Pharmacology of Ionic Channel Function: Activators and Inhibitors*, edited by Endo M, Kurachi Y, and Mishina M. Berlin: Springer, 2000, vol. 147, p. 625–649.

53. **Wang WH.** Regulation of the hyperpolarization-activated K⁺ channel in the lateral membrane of the cortical collecting duct. *J Gen Physiol* 106: 25–43, 1995.

54. **Wang W, Hebert SC, and Giebisch G.** Renal K⁺ channels: structure and function. *Annu Rev Physiol* 59: 413–436, 1997.

55. **Warth R and Bleich M.** K⁺ channels and colonic function. *Rev Physiol Biochem Pharmacol* 140: 1–62, 2000.

56. **Warth R, Hamm K, Bleich M, Kunzelmann K, von Hahn T, Schreiber R, Ullrich E, Mengel M, Trautmann N, Kindle P, Schwab A, and Greger R.** Molecular and functional characterization of the small Ca²⁺-regulated K⁺ channel (rSK4) of colonic crypts. *Pflügers Arch* 438: 437–444, 1999.

57. **Warth R, Riedemann N, Bleich M, Van Driessche W, Busch AE, and Greger R.** The cAMP-regulated and 293B-inhibited K⁺ conductance of rat colonic crypt base cells. *Pflügers Arch* 432: 81–88, 1996.

58. **Yang Y and Sigworth FJ.** Single-channel properties of I_Ks potassium channels. *J Gen Physiol* 112: 665–678, 1998.

59. **Yang Z, Xu H, Cui N, Qu Z, Chanchevalap S, Shen W, and Jiang C.** Biophysical and molecular mechanisms underlying the modulation of heteromeric Kir4.1-Kir5.1 channels by CO₂ and pH. *J Gen Physiol* 116: 33–45, 2000.